Die approbierte gedruckte Originalversion dieser Diplomarbeit ist an der TU Wien Bibliothek verfügbar
The approved original version of this thesis is available in print at TU Wien Bibliothek.

TECHNISCHE UNIVERSITÄT WIEN
Vienna University of Technology

# DIPLOMARBEIT

# Numerical analysis of the domain structure of Fe-Co-C and Co/Ni-Co films

zur Erlangung des akademischen Grades

**Diplom-Ingenieur/in**

im Rahmen des Studiums

Masterstudium Technische Physik

eingereicht von

**Sebastian Deußner**

Matrikelnummer 0925197

ausgeführt am Institut für Physik Funktioneller Materialien
der Fakultät für Physik der Universität Wien

Betreuer/in: Assoz. Prof. Dipl.-Ing. Dr. techn. Dieter Süss
Mitwirkung: Dipl.-Phys. Dr. Claas Abert

Wien, 2.9 .2020

Unterschrift Verfasser/in  Unterschrift Betreuer/in

# Contents


**1 Abstract** **2**

**2 Introduction** **2**

**3 Domain Theory** **4**

3.1 Single domain size . . . . . 4

3.2 The origin of stripe domains . . . . . 5

3.3 Analytical description of the stripe domains . . . . . 7

**4 Micromagnetism** **11**

4.1 Analytic micromagnetism . . . . . 11

4.1.1 Micromagnetic calculation of the critical thickness . . . . . 13

4.2 Numerical Micromagnetism . . . . . 16

4.2.1 Multiple period method . . . . . 17

4.2.2 One period method . . . . . 18

**5 Fe-Co-C** **19**

5.1 Simulations . . . . . 19

5.2 Multiple period simulations . . . . . 21

5.3 One period micromagnetics . . . . . 21

5.3.1 Validation of the simulation method . . . . . 25

5.4 Varying material parameters . . . . . 32

5.5 Minimal thickness for the formation of stripe patterns . . . . . 39

5.6 Analysis of experimental stray field data . . . . . 42

5.7 Simulation of a finite structure . . . . . 46

**6 Co/Ni-Co** **51**

6.1 Calculations of the critical thickness . . . . . 51

6.2 One dimensional simulation . . . . . 52

6.3 Simulating the Co/Ni-Co Structure as one layer . . . . . 55

**7 Conclusions** **60**




Die approbierte gedruckte Originalversion dieser Diplomarbeit ist an der TU Wien Bibliothek verfügbar
The approved original version of this thesis is available in print at TU Wien Bibliothek.
TU Bibliothek Your knowledge hub WIEN

Die approbierte gedruckte Originalversion dieser Diplomarbeit ist an der TU Wien Bibliothek verfügbar
The approved original version of this thesis is available in print at TU Wien Bibliothek.

# 1 Abstract

This work deals with the formation of magnetic domains in thin ferromagnetic films. It gives a short introduction to domain theory and introduces existing analytical methods for the description of narrow stripe domains. The main focus is on the numerical analysis of two alloy layers whose understanding of their magnetic behavior may lead to the development of possible new materials. The research was realized in the form of micromagnetic simulations and concentrated mainly on the static magnetic distribution of these structures. The purpose of these simulations was to reproduce and complement experiments performed by K. Leistner et al. on Co/Ni-Co films and by V. Neu et al. [1] on tetragonally distorted Fe-Co-C films. The first structure is a cobalt layer, with varying thickness, on top of four Co/Ni multi-layers. Depending on the thickness of the cobalt layer, the material has a homogeneous in-plane magnetization below a critical thickness and switches to perpendicular oriented magnetization as the thickness is getting larger. This critical thickness has been calculated to be 0.437 nm and could be verified using "magnum.fe" as the simulation software. The second set of simulations was performed on Fe-Co-C films with varying thickness in the range of 30 nm – 110 nm. For this structure, it has been found that for a thickness above 45 nm the magnetization distribution represents a stripe domain structure. The width of these stripes increases with the thickness of the sample. The dependence between the thickness of the film and the stripe width as well as the critical thickness at which the stripes appear was investigated. For this purpose a new one period simulation method was developed and tested on the basis of various experimental results. Furthermore, the influence of material parameters on the magnetization as well as the stray field above the structure was identified.

# 2 Introduction

Demand and requirements for ferromagnetic materials for high-density magnetic storage devices and electric motors have risen sharply in recent years. The recording density of hard disks, i.e. the amount of information that can be stored per unit area, has increased by more than 8 orders of magnitude since the start of their commercial use. However, this increase, which was achieved by conventionally scaling the size of the magnetic grains, will soon reach its limits [2]. As the grains become smaller

and smaller, the ratio of magnetic energy $K_u V_g$ to thermal energy $k_b T$ decreases, and thus the energy barrier that prevents spontaneous switching of spins becomes smaller, where $K_u$ is the uniaxial anisotropy constant, $V_g$ is the volume of a grain, $k_b$ is the Boltzmann constant and $T$ is the temperature. If this energy barrier is too small, data may be lost due to thermal fluctuations. In addition, a high value of saturation magnetization $M_s$ is required to allow reading the magnetic flux of the memory bits with low noise. However, the saturation magnetization must not be too high, because the energy barrier, which should be high in order not to be overcome by thermal fluctuations, has a maximum at a defined value of $M_s$ [3]. For this reason, the search for new materials with high $K_u$ and $M_s$, which would allow us to make storage media even smaller is important. Another reason why the desire for alternative magnetic materials is strong is the excessive use of rare earths in generators, e-bikes, storage decives etc.. These are largely extracted under poor working and environmental conditions and from this perpective the development of a more sustainable alternative would be highly desirable. The energy utilized by permanent magnets depends on the saturation magnetization $M_s$ and the coercivity $H_c$. In order to save energy it is necessary to use materials with high $M_s$ and $H_c$. A material that has proven to be a good candidate is Fe-Co, because it has the highest $M_s$ among all transition metal alloys [4]. However the predicted $K_u$ of body-centered cubic Fe-Co is insufficiently large for a good use in permanent magnets. Investigations have shown that the anisotropy of Fe-Co films can be improved for example by creating a body centred tetragonal Fe-Co lattice. The first part of this work investigates the magnetic properties of thin tetragonally distorted Fe-Co films which have been additionally enhanced by cobalt. It was found that for thin Fe-Co-C layers exceeding a certain thickness, a spin reorientation phase occurs in which the magnetization changes from an in-plane state to a state with stripe domains. These stripe domains can be found in various films with perpendicular anisotropy [5–8]. The period of these stripe domain patterns increases with the thickness of the film. Until this time there is no universal analytical theory to describe the relationship between the stripe domain and thickness. Therefore numerical simulations based on the micromagnetic theory were used to get a greater understanding of this observation. The simulations have been made in comparison and collaboration with experimental investigations of these Fe-Co-C films and complement these.



Die approbierte gedruckte Originalversion dieser Diplomarbeit ist an der TU Wien Bibliothek verfügbar
The approved original version of this thesis is available in print at TU Wien Bibliothek.
TU Bibliothek Your knowledge hub WIEN

# 3 Domain Theory

The magnetic dipoles in ferromagnetic materials tend to align in the same direction even without an external field. However, areas may arise within which the magnetization is uniformly aligned in one direction, but the areas themselves differ from one another by their magnetizations direction. The formation of these so-called domains can represent an energetic advantage over a uniformly saturated structure. Small particles must exceed a certain length in order to gain an energy advantage through the formation of magnetic domains.

## 3.1 Single domain size

This section examines this minimum size for materials with uniaxial anisotropy, which rises a contribution to the magnetic energy that favors a magnetization along one specific axis. For sizes smaller than the single domain size, a domain configuration is unstable. In order to estimate this critical size an expression of the magnetic energy of a structure that forms domains must first be created. The energy of a domain wall can be expressed with a size-independent specific energy $\gamma_\mathrm{w}$ [9] which also considers the anisotropy energy and the exchange energy (Sec. 4). The area of a domain wall $F_\mathrm{w}$ can be measured with the parameter $f_\mathrm{w} = F_\mathrm{w}/V^{2/3}$, where $V$ is the volume of the particle. The domain itself has a stray field energy of $E_\mathrm{d}$, which can be represented with the dimensionless parameter $\epsilon_\mathrm{d} = E_\mathrm{d}/(VK_\mathrm{d})$, where $K_\mathrm{d}$ is the stray field energy coefficient. Consequently the total energy in units of $K_\mathrm{d}$, without the presence of an external field can be written as:

$$\epsilon_\mathrm{tot} = e_\mathrm{tot}/K_\mathrm{d} = \epsilon_\mathrm{d} + (f_\mathrm{w}/l_\mathrm{p})(\gamma_\mathrm{w}/K_\mathrm{d}), \tag{1}$$

where $l_\mathrm{p} = V^{1/3}$ is the effective particle size. The second term of Eq. (1) is decreasing with the particle size. Equating Eq. (1) with the reduced energy $N$ of a uniformly magnetized particle, furnishes a term for the single domain size $l_\mathrm{SD}$.

$$l_\mathrm{SD} = \frac{f_\mathrm{w}}{N - \epsilon_\mathrm{d}} \frac{\gamma_\mathrm{w}}{K_\mathrm{d}} \tag{2}$$

The single domain size is therefore determined on the ratio between the wall energy and the stray field. Further $l_\mathrm{SD}$ depends on the interplay of the exchange energy and the stray field energy, as the exchange energy enters the equation through the wall energy. Thereby the exchange energy prefers a uniform magnetization whereas the stray field



Die approbierte gedruckte Originalversion dieser Diplomarbeit ist an der TU Wien Bibliothek verfügbar
The approved original version of this thesis is available in print at TU Wien Bibliothek.
TU Bibliothek Your knowledge hub WIEN

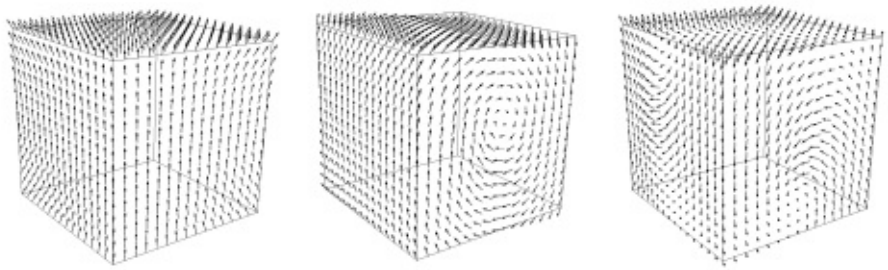

(a) (b) (c)

Figure 1: Magnetic states of Fe-Co-C cubes with different sizes. The transition between the flower state (a) and the vortex state (b) is energetically favored when the side length exceeds the single domain size. In the third state (c) another vortex appears, the state is therefore called three domain state. The structures are simulated with the simulation software magnum.fd [10].

energy prefers the formation of domains. For materials with low anisotropy it has been shown that the single domain size scales with the exchange length $\Delta_\mathrm{d} = \sqrt{A/K_\mathrm{d}}$ [9], where $A$ is the exchange constant. For cubes with a side length smaller than the single domain size, the magnetization prefers a flower state (Fig. 1a). In this state, the magnetic moments point in the direction of the easy axis, but are slightly curved outwards at the edges of the cube. As the length is increased above $l_\mathrm{SD}$, a vortex state (Fig. 1b) is energetically favoured. The vortex state is meta-stable below $l_\mathrm{SD}$, as well as the flower state is meta-stable in a small range above that length. A third meta-stable state is a state called the three domain state, where a second vortex appears (Fig. 1c). In literature values from $l_\mathrm{SD} = 6.8\Delta_\mathrm{d}$ for $Q = 0.02$ [11] [12] up to $l_\mathrm{SD} = 10.8\Delta_\mathrm{d}$ for uniaxial cobalt with $Q = 0.4$ [13] can be found, where $Q = K/K_\mathrm{d}$ and $K$ is the appropriate anisotropy constant.

## 3.2 The origin of stripe domains

This chapter gives an overview of the origin of stripe domains as found in some thin films with perpendicular anisotropy, without getting into the detail of quantitative aspects. To understand the origin of stripe domains which are often found in thin films one first have to look at bulk structures. The direction of the magnetization is determined by three energy contributions, anisotropy energy, exchange energy and



Die approbierte gedruckte Originalversion dieser Diplomarbeit ist an der TU Wien Bibliothek verfügbar
The approved original version of this thesis is available in print at TU Wien Bibliothek.
TU Bibliothek Your knowledge hub WIEN

demagnetization energy. A closer look at these contributions is given in Sec. 4. If an easy axis in the direction of the z-axis is assumed, the anisotropy energy punishes a magnetization in y- and x- direction. On the other hand, the stray field energy punishes a large stray field outside the sample. If the uniaxial anisotropy is strong enough to overcome the shape anisotropy, which favours in-plane magnetization, the combination of uniaxial anisotropy and stray field minimization results in a periodic oscillation of domains with magnetization in positive and negative z-direction. In comparison to a uniformly saturated structure, this periodic sequence reduces the magnetic energy $(1/2)\int \mu_0 \boldsymbol{H}^2 dV$ [14] by a factor of $1/N$, where $N$ is the number of domains formed. However, the exchange energy favors a low oscillation frequency, since each domain wall brings an additional energy contribution. In the interior, the regularizing effect of the exchange energy is more dominant [15] leading to the effect of domain branching, where the structure has wide domains on the inside which split into narrower ones on the surface. Figure 2 shows a sketch of the domain branching effect. For materials with low perpendicular anisotropy and especially for materials with an additional cubic anisotropy term another surface effect appears. The domains form a closed structure to complete the flux circuit and prevent a stray field outside the sample (Sketch 3). The domains with misoriented magnetization with respect to the easy axis increase the anisotropy energy. For materials with only uniaxial anisotropy, no strict domain walls are formed and the closure configuration is continuous [9]. When we transition from a bulk structure to a thin film, the inner area becomes smaller and smaller until the two surfaces join together. Therefore, thin films have narrow parallel stripe domains that are for some parts misoriented. In thin films, the area of misoriented magnetization is not limited to the surface as with thick materials, but occupies a non-negligible region, as can be seen in Fig. 11. The wall between two stripes, which represents a switch from domains with positive $M_\mathrm{z}$ to domains with negative $M_\mathrm{z}$ or vice versa, occurs within the plane perpendicular to the stripes. This behavior is described by a Néel wall. It turns out that the direction of magnetization is not only limited to the cross-section normal to the stripes. In addition, the magnetic moments are tilted in the direction of the stripes. When looking at only a few adjacent stripes, they are approximately parallel and uniformly tilted in the same direction. As the film dimension is getting bigger, global domains specified by this tilt are formed (Fig. 31. These domains also tend to form closed structures similar to Fig. 3 to minimize the stray field energy. In



Die approbierte gedruckte Originalversion dieser Diplomarbeit ist an der TU Wien Bibliothek verfügbar
The approved original version of this thesis is available in print at TU Wien Bibliothek.
TU Bibliothek Your knowledge hub WIEN

contrast to the domain walls between the individual stripes, so-called Bloch walls are formed between these global domains.

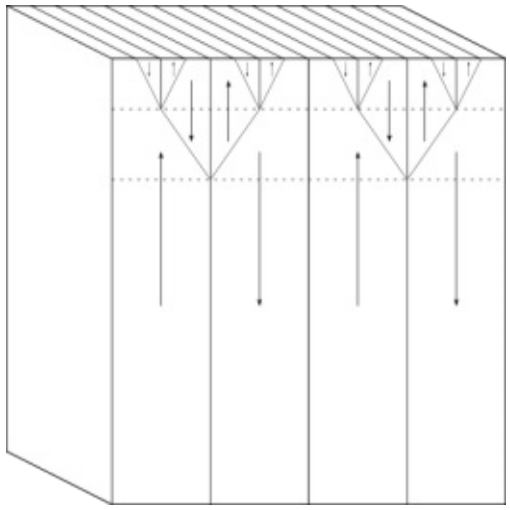

Figure 2: Domain branching in a ferromagnetic material with uniaxial perpendicular anisotropy [15].

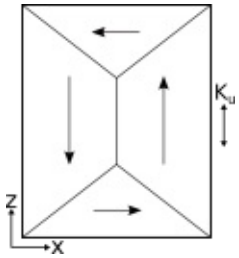


Figure 3: Closure domains are formed to minimize the stray field energy.

## 3.3 Analytical description of the stripe domains

The first steps to describe the domain structure of thin ferromagnetic films with perpendicular easy axis were taken by Kittel [14] in 1946. He considered the energy of different magnetic configurations of thin films, which were a closed and an open flux configuration, as well as an in-plane magnetization configuration (Fig. 4). He found that at a thickness less than a certain value, the case of a film which is magnetized uniformly in the plane has the lowest energy. For a greater thickness, the closed flux configuration is preferred. The case of an open flux only occurs for a very large



Die approbierte gedruckte Originalversion dieser Diplomarbeit ist an der TU Wien Bibliothek verfügbar
The approved original version of this thesis is available in print at TU Wien Bibliothek.
TU Bibliothek Your knowledge hub WIEN

anisotropy. By minimizing the total magnetic energy of the closed flux configuration

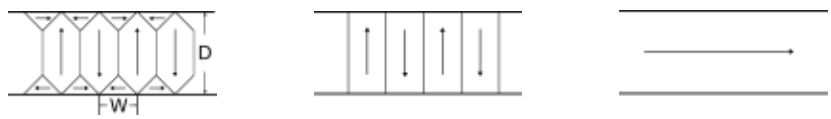


(a) (b) (c)

Figure 4: Domain configurations considered by Kittel [14]. The figure shows a closed flux configuration (a), an open flux configuration (b) and a single domain state with a magnetization in direction of the plane (c).

he calculated the dependency of the thickness $D$ of the film and the domain width $W$. In his calculations he derives a root dependence of $W$ and $D$ which is:

$$W = \sqrt{2\sigma_w D/\rho_\alpha}, \tag{3}$$

where $\sigma_w$ is the surface energy density of a Bloch wall and $\rho_\alpha$ is the anisotropy energy density [14]. As an expression for the demagnetization energy of the film, he took twice the value for one surface of an infinitely thick film. Thus he neglected the dipole interaction of the two surface poles of a film, whereby Eq. (3) is only given as an approximation for large thicknesses [16]. Later Málek and Kamberský [17] derived a more accurate expression for the areal density of the demagnetization energy which also includes the limit of very thin thicknesses which is:

$$F_{\text{demag}} = \frac{4J_{\text{s}}^2 W}{\mu_0 \pi^3} \sum_n^\infty \frac{1}{n^3} \left(1 - e^{-\frac{n\pi D}{W}}\right), \tag{4}$$

where $J_{\text{s}}$ is the magnetic saturation polarization and $\mu_0$ is the vacuum permeability. For an infinitely thick film, Eq. (4) becomes the expression chosen by Kittel [14]. With $F_{\text{wall}} = \gamma D/W$ being the domain wall contribution for the stripe pattern configuration, where $\gamma$ is the surface density of the energy of a wall, the total energy related to unit surface of a film is given by $F_{\text{tot}} = F_{\text{demag}} + F_{\text{wall}}$. The minimization of the energy for a given thickness of the film $\partial F_{\text{tot}}/\partial W = 0$, raises the condition:

$$\frac{4J_{\text{s}}^2}{\mu_0 \pi^3} W^2 \sum_n^\infty \frac{1}{n^3} \left[1 - e^{-\frac{n\pi D}{W}} \left(1 + \frac{n\pi D}{W}\right)\right] - \gamma D = 0 \tag{5}$$

The numerical solution of this equation, with for example Newton's method, leads to the dependence $W = W(D)$. The validity of the determination of $W(D)$ from Eq. (5) was verified in comparison with experimental data of MnBi films [17]. However, the



Die approbierte gedruckte Originalversion dieser Diplomarbeit ist an der TU Wien Bibliothek verfügbar
The approved original version of this thesis is available in print at TU Wien Bibliothek.
TU Bibliothek Your knowledge hub WIEN

domain-wall width $\delta_{\mathrm{w}}$ is neglected in their description. Although the domain walls in MnBi are indeed very narrow, they cannot be neglected for ultra thin films where $\delta_w \gg D$ [18]. An analytical approach to determine an expression for $W = W(D)$ is given by Millev via expansions of the Bose–Einstein integrals [16]. With a term of the demagnetization energy analog to [17] he calculated an expression for the domain width, which is [18]:

$$W = \frac{\pi D}{2\sqrt{e}} \exp\left(\frac{\pi\gamma}{\mu_0 M_{\mathrm{s}}^2 D}\right) \tag{6}$$

where $M_{\mathrm{s}}$ is the saturation magnetization. Equation 6 as well as the solution of Eq. (5) predict that $W$ will decrease as $D$ increases in the ultra thin regime. In some cases, the methods described above have been able to describe the experimentally obtained behavior of domain widths as a function of the film thickness to a certain extent. Brandenburg et al. compared experimental values for cobalt films with calculations from Eq. (5) and found that the calculated values of the domain width are too low [7]. Moreover, the behavior predicted by the theory in the ultra-thin regime could not be observed in the experiments as underneath a certain critical thickness the magnetization was uniformly in-plane. This comparison to the analytic theory can be seen in Fig. 5. For the analytical evaluation they used the material parameters $K_1 = 0.45$ mJ/m$^3$, $J_{\mathrm{s}} = 1.8$ T and $A = 28 \times 10^{-12}$ J/m. Another group [6] was able to compare experimental data of a Co-Pt film (Fig. 6) with an analytical expression of $W(D)$ which, analogous to Kittel, specifies a root dependence of $W$ and $D$. However a further comparison is not possible, as at present no universal theory of the stripe domain width as a function of the film thickness is available [7]. For this reason, it is necessary to use a more universal theory for a better understanding of the domain structure of thin ferromagnetic layers. The micromagnetic theory perfectly serves this purpose and is discussed in detail in the next section.



Die approbierte gedruckte Originalversion dieser Diplomarbeit ist an der TU Wien Bibliothek verfügbar
The approved original version of this thesis is available in print at TU Wien Bibliothek.
TU Bibliothek Your knowledge hub WIEN

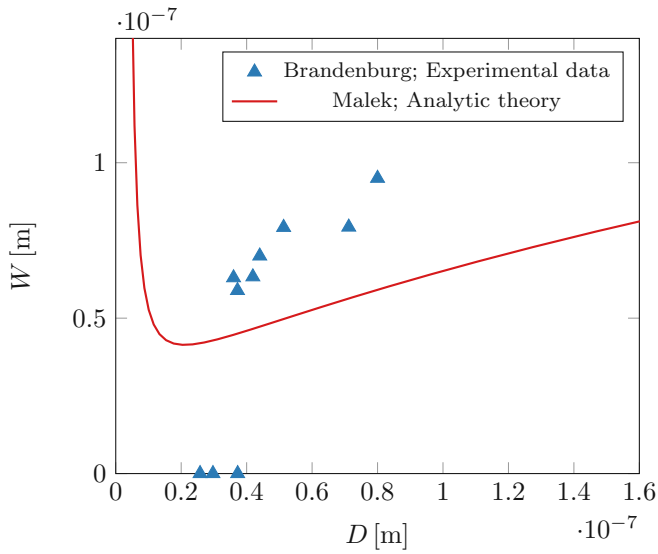


Figure 5: Stripe domain width as a function of the film thickness for a thin cobalt film. The blue triangles represent the experimentally measured data [7], while the red line is the solution of (5). The case of non-existent stripe domains, is displayed with a $W$ of zero.

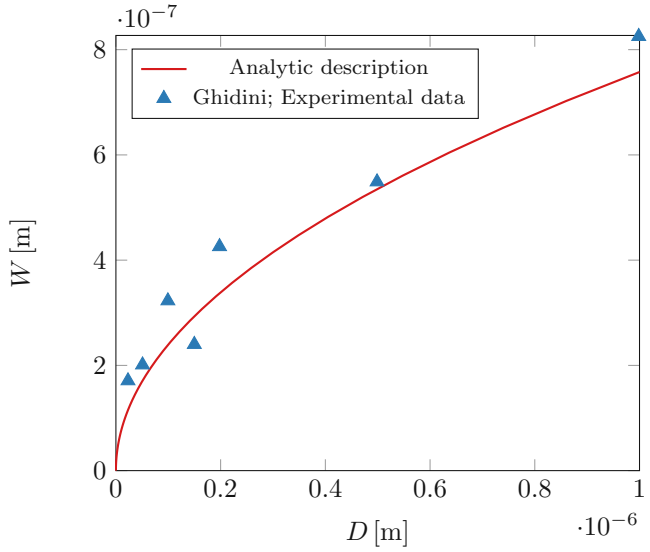


Figure 6: Stripe domain width as a function of the film thickness for a Co-Pt film. The experimental data measured by [6] is indicated by blue triangles. The red line is calculated with an analytic expression predicting a square root dependency for $W(D)$ [6].



Die approbierte gedruckte Originalversion dieser Diplomarbeit ist an der TU Wien Bibliothek verfügbar
The approved original version of this thesis is available in print at TU Wien Bibliothek.
TU Bibliothek Your knowledge hub WIEN

# 4 Micromagnetism

The theory of micromagnetism is a model to describe the magnetic distribution of magnetic materials and has its applications among others in the design and development of magnetic devices. In contrary to an atomic level theory, which uses quantum mechanic calculations, micromagnetism uses a continuous description of the magnetization, but still extends the classical field theory by non-classical effects like the exchange interaction [19]. It allows to resolve the inner structure of domain walls and vortices, while still enable the numerical calculations for relatively large system sizes. Therefore the theory has proven to be a good model for describing systems with a length scale of $1 - 1000$ nm.

## 4.1 Analytic micromagnetism

The main assumption of micromagnetism is a continuous magnetization $\boldsymbol{M}(\boldsymbol{x})$ which has a constant norm at any point and can be written in terms of the unit vector field $\boldsymbol{m}$:

$$\boldsymbol{M}(x) = M_\mathrm{s}\,\boldsymbol{m}(x) \quad \text{with} \quad |\boldsymbol{m}(\boldsymbol{x})| = 1. \tag{7}$$

With this constraint, micromagnetic calculations can be used to determine the spatial magnetization distribution of a magnetic material. Therefore the solution is required to further fulfill the constraint of minimal magnetic energy with respect to its magnetization. In the theory of micromagnetism this energy is composed of the following components:

$$E_\mathrm{tot} = E_\mathrm{exch} + E_\mathrm{demag} + E_\mathrm{aniso} + E_\mathrm{Zeeman}, \tag{8}$$

where the four contributions to the magnetic energy are the exchange energy $E_\mathrm{exch}$, the demagnetization energy $E_\mathrm{demag}$, the anisotropy energy $E_\mathrm{aniso}$ and the Zeeman energy $E_\mathrm{Zeeman}$. The exchange energy is a result of the quantum mechanical exchange interaction which is caused by the Coulomb energy of two indistinguishable particles with overlapping wavefunctions. This interaction favours a parallel spin orientation and is the reason of spontaneous magnetization in ferromagnetic materials. The exchange energy can be expressed with [9],

$$E_\mathrm{exch} = A \int_V (\nabla \boldsymbol{m})^2 \mathrm{d}V \tag{9}$$



Die approbierte gedruckte Originalversion dieser Diplomarbeit ist an der TU Wien Bibliothek verfügbar
The approved original version of this thesis is available in print at TU Wien Bibliothek.
TU Bibliothek Your knowledge hub WIEN

where $V$ is the volume of the system and $\boldsymbol{m}$ is the magnetization direction vector. The demagnetization field is generated by the dipole-dipole interactions of the elementary magnets of magnetic materials. It has the effect to reduce the total magnetic moment of the system. An expression of the associated demagnetization energy is given with,

$$E_{\mathrm{demag}} = -\frac{\mu_0}{2} \int_V \boldsymbol{M}\boldsymbol{H}_{\mathrm{d}}(\boldsymbol{M})\mathrm{d}V, \tag{10}$$

where $\boldsymbol{H}_{\mathrm{d}}$ is the demagnetization field. The anisotropy field favours the alignment of the magnetic moments of ferromagnetic materials in direction of a certain axis and is a result of spin-orbit interactions. A material can have one or more so called easy axes. The direction of these easy axes depends on the crystal structure of the material. In case of only one easy axis as found in hexagonal and tetragonal crystals, the energy contribution of the anisotropy field is given by

$$E_{\mathrm{aniso}} = -\int_V K_{\mathrm{u}}(\boldsymbol{m}\,\boldsymbol{e}_{\mathrm{u}})^2 + \mathcal{O}(\boldsymbol{m}^4)\,\mathrm{d}V \tag{11}$$

where $K_{\mathrm{u}}$ is the uniaxial anisotropy constant and $\boldsymbol{e}_{\mathrm{u}}$ is the unit vector parallel to the easy axis. The last contribution to the total magnetic energy, the so called Zeeman energy

$$E_{\mathrm{Zeeman}} = -\mu_0 \int_V M_{\mathrm{s}}\boldsymbol{m}\,\boldsymbol{H}_{\mathrm{ext}}\,dV \tag{12}$$

is the interaction between the magnetization and an external field $\boldsymbol{H}_{\mathrm{ext}}$. To be a stable micromagnetic state, the total energy has to be minimized with respect to the magnetization $\boldsymbol{m}$. Additionally the solution has to fulfill the unit-sphere constraint (7). Because $\boldsymbol{m}$ is a continuous vector field, the minimization of $E(\boldsymbol{m})$ can be done by variational calculus. This yields an expression for the differential $\delta E$ which is

$$\delta E(\boldsymbol{m}, \boldsymbol{v}_m) = \int_{\Omega_m} \frac{\delta E}{\delta \boldsymbol{m}} \cdot \boldsymbol{v}_{\mathrm{m}} + \int_{\partial\Omega_m} \boldsymbol{R} \cdot \boldsymbol{v}_m\,d\boldsymbol{s}, \tag{13}$$

where $\boldsymbol{v}_m$ is an arbitrary test function, $\boldsymbol{R}$ is the boundary term of the functional derivative of the energy, $\Omega_m$ is the magnetic volume and $\partial\Omega_m$ is the respective interface. Condition (7) can be included in the calculation via Lagrange multipliers which results in the condition of $\delta E/\delta\boldsymbol{m}$ and $\boldsymbol{m}$ being parallel and hence

$$\boldsymbol{m} \times \frac{\delta E}{\delta \boldsymbol{m}} = 0 \tag{14}$$

which is Brown's condition [20]. The calculation further yields the boundary condition

$$\boldsymbol{m} \times \boldsymbol{R} = 0. \tag{15}$$



Die approbierte gedruckte Originalversion dieser Diplomarbeit ist an der TU Wien Bibliothek verfügbar
The approved original version of this thesis is available in print at TU Wien Bibliothek.
TU Bibliothek Your knowledge hub WIEN

The energy differentials and boundary terms can be calculated separately for each energy contribution in Eq. (8). Therefore variations of the energy terms (9 - 12) are compared with Eq. (13) [19]. The following equations are the resulting derivative and boundary terms of the individual energy contributions.

$$\frac{\delta E_{\text{exch}}}{\delta \boldsymbol{m}} = -2\nabla \cdot (A\nabla \boldsymbol{m}), \qquad \boldsymbol{R} = 2A\frac{\partial \boldsymbol{m}}{\boldsymbol{n}} \quad \text{Exchange energy} \tag{16}$$

$$\frac{\delta E_{\text{demag}}}{\delta \boldsymbol{m}} = -\mu_0 M_{\text{s}} \boldsymbol{H}_{\text{d}}, \qquad \boldsymbol{R} = 0 \quad \text{Demagnetization energy} \tag{17}$$

$$\frac{\delta E_{\text{aniso}}}{\delta \boldsymbol{m}} = -2K_1 \boldsymbol{e}_{\text{u}}(\boldsymbol{e}_{\text{u}} \cdot \boldsymbol{m}), \qquad \boldsymbol{R} = 0 \quad \text{Uniaxial anisotropy energy} \tag{18}$$

$$\frac{\delta E_{\text{Zeeman}}}{\delta \boldsymbol{m}} = -\mu_0 M_{\text{s}} \boldsymbol{H}_{\text{Zeeman}}, \qquad \boldsymbol{R} = 0 \quad \text{Zeeman energy} \tag{19}$$

In the theory of micromagnetism the time evolution of $\boldsymbol{m}$ is described with the Landau-Lifshitz-Gilbert (LLG), which is in its explicit form

$$\partial_t \boldsymbol{m} = -\frac{\gamma_{\text{g}}}{1+\alpha^2}\boldsymbol{m} \times \boldsymbol{H}_{\text{eff}} - \frac{\alpha\gamma_{\text{g}}}{1+\alpha^2}\boldsymbol{m} \times (\boldsymbol{m} \times \boldsymbol{H}_{\text{eff}}), \tag{20}$$

where $\gamma_{\text{g}}$ is the reduced gyromagnetic ratio and $\alpha$ is the damping parameter. The effective field $\boldsymbol{H}_{\text{eff}}$ which can be defined as $\boldsymbol{H}_{\text{eff}} = -\frac{1}{\mu_0 M_{\text{s}}}\frac{\delta E}{\delta \boldsymbol{m}}$, considers contributions of exchange, anisotropy and demagnetization energy as well as an external field. For a constant field, the trajectory of the magnetization as described by the LLG is the combination of a precessional motion around the effective field and a dissipative motion towards $\boldsymbol{H}_{\text{eff}}$. Because of the reason that the micromagnetic equations are complicated non-linear equations, they are difficult to solve analytically. Therefore, numerical solutions of the micromagnetic equations is the method of choice for most problems. A short introduction of the most common methods for solving the micromagnetic equations numerically are given in Sec. 4.2.

### 4.1.1 Micromagnetic calculation of the critical thickness

This chapter shows a micromagnetic approach of the calculation of the minimal thickness $D_{\text{cr}}$, which a ferromagnetic material with low perpendicular anisotropy ($Q = K_{\text{u}}/K_{\text{d}} < 1$) has to exceed in order to form stripe domains as described in Sec. 3.2. To calculate $D_{\text{cr}}$, one has to start with the micromagnetic equations which



Die approbierte gedruckte Originalversion dieser Diplomarbeit ist an der TU Wien Bibliothek verfügbar
The approved original version of this thesis is available in print at TU Wien Bibliothek.
TU Bibliothek Your knowledge hub WIEN

can be written in the form [9]:

$$\boldsymbol{m} \times (2A\Delta\boldsymbol{m} + 2K_1\boldsymbol{e}_\mathrm{z}(\boldsymbol{e}_\mathrm{z}\boldsymbol{m}) + J_\mathrm{s}H_\mathrm{ex}\boldsymbol{e}_\mathrm{y} - J_\mathrm{s}\,\nabla\Phi_\mathrm{d}) = 0, \tag{21}$$

where and $\boldsymbol{e}_\mathrm{i}$ are the unit vectors and with $\boldsymbol{H}_\mathrm{d} = -\nabla\Phi_\mathrm{d}$. The first term in brackets is a simplification of the exchange term for constant $A$. The external field $H_\mathrm{ext}$ is set along the y-axis parallel to the stripes and $m_\mathrm{z}$ is the magnetization component in the direction of the easy axis. With the simplification $\boldsymbol{m}$ and $\Phi_\mathrm{d}$ being small and with $\Delta\Phi_\mathrm{d} = (J_\mathrm{s}/\mu_0)\,\nabla\cdot\boldsymbol{m}$, Eq. 21 leads to the following set of differential equations [9]:

$$\begin{aligned} &-2A\Delta m_\mathrm{z} - 2K_\mathrm{u}m_\mathrm{z} + J_\mathrm{s}H_\mathrm{ext}m_\mathrm{z} + J_\mathrm{s}\frac{\partial\Phi_\mathrm{d}}{\partial z} = 0, \\ &2A\Delta m_\mathrm{x} - J_\mathrm{s}H_\mathrm{ex}m_\mathrm{x} - J_\mathrm{s}\frac{\partial\Phi_\mathrm{d}}{\partial x} = 0, \\ &\Delta\Phi_\mathrm{d} = \left(\frac{J_\mathrm{s}}{\mu_0}\right)\left(\frac{\partial m_\mathrm{x}}{\partial x} + \frac{\partial m_\mathrm{z}}{\partial z}\right), \Delta\widetilde{\Phi}_\mathrm{d} = 0, \end{aligned} \tag{22}$$

where $\widetilde{H}_\mathrm{d}$ stands for the stray field outside the film. The component $m_\mathrm{z}$ was treated constant ($= 1$) to first order. The boundary conditions are:

$$\begin{aligned} &\Phi_\mathrm{d} = \widetilde{\Phi}_\mathrm{d}, \frac{\partial m_\mathrm{x}}{\partial z} = \frac{\partial m_\mathrm{z}}{\partial z} = 0, \\ &\frac{\partial\widetilde{\Phi}_\mathrm{d}}{\partial z} - \frac{\partial\Phi_\mathrm{d}}{\partial z} = -\frac{J_\mathrm{s}m_\mathrm{z}}{\mu_0} \quad \text{for} \quad z = \pm\frac{D}{2} \end{aligned} \tag{23}$$

The differential equations (22) can be solved rigorously with a waveform ansatz for $m_\mathrm{x}$, $m_\mathrm{z}$, $\Phi_\mathrm{d}$ and $\widetilde{\Phi}_\mathrm{d}$ [9]. The solution leads to sinusoidal, stripe-shaped deviations of a magnetization initially along the field, which depend only on the film thickness, the external field and the parameter $Q$. The thickness of the film enters through the boundary conditions. The lowest possible critical thickness in a given field can be found by optimizing the wavenumber of the waveform ansatz and is given in Fig. 7, while the critical stripe width can be retained from Fig. 8.

For materials with $Q < 0.1$ and with no external field, the critical thickness is roughly as thick as a Bloch wall and has a value of $D_\mathrm{cr} = 2\pi\sqrt{A/K_\mathrm{u}}$ [21]. The stripe width at this thickness is as big as the thickness itself. For $Q$ values greater than 0.1 the critical thickness as well as the ratio $D_\mathrm{cr}/W_\mathrm{cr}$ is decreasing with $Q$. The red dot in Figure 7 and 8 indicates the $Q$ value of 0.228 for a Fe-Co-C multilayer. According to the graphs and with $A = 28\times10^{-12}$ J/m and $K_1 = 0.4\times10^6$ J/m$^3$, this $Q$ value leads to $D_\mathrm{cr} = 42.4$ nm and $W_\mathrm{cr} = 48.8$ nm.



Die approbierte gedruckte Originalversion dieser Diplomarbeit ist an der TU Wien Bibliothek verfügbar
The approved original version of this thesis is available in print at TU Wien Bibliothek.
TU Bibliothek Your knowledge hub WIEN

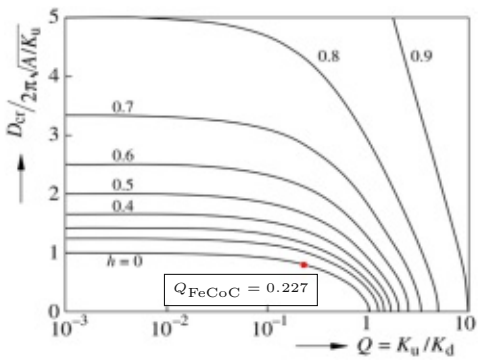


Figure 7: Critical thickness $D_{\mathrm{cr}}$ at which the stripe domains first occurs versus the material parameter $Q$ [9]. The red dot indicates the $Q$ value of Fe-Co-C and is used in Sec. 5.5 to compare this result for $H_{\mathrm{ext}} = 0$ with the critical thickness from one period micromagnetic calculations.

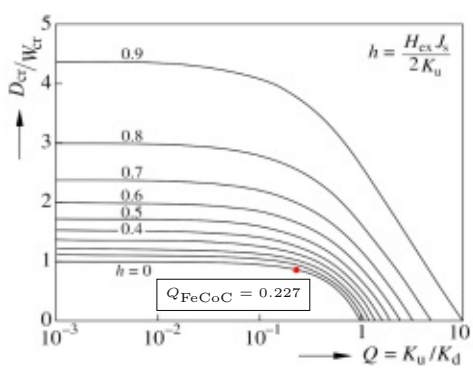


Figure 8: Inverse stripe domain width $W_{cr}$ at the critical thickness versus $Q$ [9]. The red dot again indicates the $Q$ value for Fe-Co-C.



Die approbierte gedruckte Originalversion dieser Diplomarbeit ist an der TU Wien Bibliothek verfügbar
The approved original version of this thesis is available in print at TU Wien Bibliothek.
TU Bibliothek Your knowledge hub WIEN

## 4.2 Numerical Micromagnetism

For most problems, the solution of the partial differential equations from Sec. 4 is only possible by going from analytical to numerical micromagnetism. A general basis of numerical or discrete micromagnetism is the assumption that neighbouring magnetic dipoles in magnetic materials can only differ slightly from each other due to strong exchange forces and can be approximated to be parallel. Discrete and further numerical micromagnetics uses this property to divide the solid into discrete areas of uniform magnetization. However, they involve high computational effort, which mainly results from the calculation of the demagnetization field and the exchange energy. The calculation of the demagnetization field, which is characterized by a long-range interaction, has a complexity of $\mathcal{O}(N^2)$ with $N$ being the number of simulation cells, when implemented naively [19], but can be improved to $\mathcal{O}(N \log N)$ with for example the finite-element method [22] and to $\mathcal{O}(N)$ with multipole expansion [23]. Although the exchange interaction is only local, it also increases the computational complexity due to its second order in space and a resulting local coupling with high stiffness. The first step in solving a micromagnetic problem, is the calculation of the effective field $\boldsymbol{H}_{\text{eff}}$ and the respective energy contributions. In most cases this happens with the discretization of space. Then either the energy has to be minimized or the time evolution of $\boldsymbol{m}$ must be computed according to the LLG. The most common methods for the spatial discretization are the finite-difference method (FDM) [24] and the finite-element method (FEM). In both methods the body of the magnetic structure is subdivided into a mesh of cells. The form of the cells of this mesh is different for the two methods, whereas in both cases the cell size has to be chosen small enough to accurately resolve the structure of domain walls. The characteristic length of a domain wall is determined by the exchange length $\Delta_{\text{d}}$. A cell which is too small, however, results in an unnecessarily large calculation effort. The FDM subdivides the magnetic body into a regular cuboid mesh. This restriction to regular cells leads to fast algorithms but can be an obstacle for complex geometries. In contrary the mesh in the FEM consists of irregular tetrahedral cells and is therefore more flexible. In both methods, the computational complexity of calculating the demagnetization field can be reduced to $\mathcal{O}(N \log N)$ [19]. The subsequent solution of the time development by means of LLG can be done for example by the Runge Kutta [25] method. An energy minimization as it is required, for example in the calculation of hysteresis



Die approbierte gedruckte Originalversion dieser Diplomarbeit ist an der TU Wien Bibliothek verfügbar
The approved original version of this thesis is available in print at TU Wien Bibliothek.
TU Bibliothek Your knowledge hub WIEN

curves, is generally performed iteratively based on gradient evaluations. The simplest algorithm for this is the steepest-descent method. When starting from a specific magnetization state, this method allows the calculation of the nearest minimum which is indispensable for hysteresis curves.

Within the first part of this work numerical micromagnetism is used to investigate stripe domain structures, in form of micromagnetic simulations performed with the simulation software magnum.fd [10]. Therefore a multiple period method from [26] as well as a specially designed one period method is applied and compared for advantages. For simulations with magnum.fd the structure must be created in the desired dimensions and meshed into individual cubic cells of the same size. Since the magnetization is constant in each individual cell, its size must not be too large to ensure the functionality of the simulation. If, however, constant magnetization in one or more directions in space is expected based on previous observations, the cells can be chosen accordingly to allow a shorter simulation time. Therefore their size has to be chosen appropriately depending on the simulated structure.

### 4.2.1 Multiple period method

Since experimental measurements of stripe domain structures [1], revealed a homogeneous magnetization along the stripes for a relatively wide area, the simulated structure in this direction does not have to be explicitly resolvable over a large range for this method. For this reason, a rod-like shape with a certain height and length is chosen as the structure, which results in an infinitely extended film in the direction of the stripes when using periodic boundary conditions (PBC) in this direction. In PBC, copies of the structure itself are periodically linked together so that an exit at one end of the structure leads to a re-entry at the other side. This creates the effect of an infinitely extended structure which is achieved with relatively low computational effort. The implementation of the PBC for the calculation of the exchange field differs from the one used in the calculation of the stray field field. The calculation of the exchange field with PBC is realized by taking the first cell of the structure as the successor of the last cell. To determine the stray field with PBC, some few copies of the structure are attached to the structure itself in both directions. Then the stray field of the middle structure is calculated. To imitate an experimental set-up with a saturated magnetization, the starting magnetization is set to be in-plane. The time



Die approbierte gedruckte Originalversion dieser Diplomarbeit ist an der TU Wien Bibliothek verfügbar
The approved original version of this thesis is available in print at TU Wien Bibliothek.
TU Bibliothek Your knowledge hub WIEN

integration of the magnetization with the consideration of exchange field, anisotropy field and the demagnetization field and without the presence of an external field, now leads to sinusoidal waves across the structure. The thickness of this structure can be ramped up to analyse its effect on the wavelength of the stripe domains. The wavelength can be calculated using either fast Fourier transformation or simply by calculating the number of periods over a specific length.

### 4.2.2 One period method

The new method for calculating the stripe width should have two decisive advantages over the method described in Sec 4.2.1. It should no longer be dependent on the x length of the simulated structure and show whether the calculated width actually belongs to the global energy minimum. For this only very short cuboids are simulated, whose x dimension is approximately in the range of the expected single period length. The thickness is increased again over a certain range, but for each thickness several measurements with slightly different x lengths are carried out. If the relaxed magnetization on this short distance forms exactly one full period of a wave, the optimal period length can be determined by calculating and comparing the energy densities of the individual short cuboids with different lengths. The length of the structure having the lowest energy density may be taken as the correct period to that particular thickness. For each set of simulations, $\mathrm{L_x}$ is increased in the range of some nanometers around the expected period. The set-up is a cubic mesh with a single cell in the direction of the y-axis but with a fine mesh in the z-axis direction. In the direction of the x-axis, the cell size for the shortest structure length $\mathrm{L_x}$ of a simulation set is always set to 1 nm and then stretched while $\mathrm{L_x}$ is increased. The calculations are performed with periodic boundary conditions in the y and x directions. As a simulation starting point, the magnetization component $m_\mathrm{y}$ is set to be 0.86 while $m_\mathrm{x}$ is 0. The magnetization perpendicular component $m_\mathrm{z}$ is set to be $+0.5$ for $x \leq \frac{\mathrm{L_x}}{2}$ and $-0.5$ for $x > \frac{\mathrm{L_x}}{2}$, which steers the magnetization to form a single waveform. Then the structure is relaxed considering demagnetization, exchange and anisotropy field. The magnetization of the relaxed result is used as the start configuration of the next $\mathrm{L_x}$ step to provide a faster simulation time. After simulating a set of structures with different $\mathrm{L_x}$ lengths and measuring their energy density a plot of $E/V$ vs $\mathrm{L_x}$ can be generated. The energy minimum of this plot will indicate the stripe period of the specific material.



Die approbierte gedruckte Originalversion dieser Diplomarbeit ist an der TU Wien Bibliothek verfügbar
The approved original version of this thesis is available in print at TU Wien Bibliothek.
TU Bibliothek Your knowledge hub WIEN

# 5 Fe-Co-C

As mentioned before, the material first examined in this work is a tetragonally distorted Fe-Co-C film. Here, this ferromagnetic material with perpendicular anisotropy shall be investigated with the above mentioned analytical methods. Experiments have shown that in thin Fe-Co-C layers with a thickness in the two to three-digit nanometer range, the magnetization shows narrow stripe domains as described in Sec. 3.2. The experimentally determined material parameters are $M_\mathrm{s} = 2.1/\mu_0$ T, $A = 28 \times 10^{-12}$ J/m and $K_1 = 0.4 \times 10^6$ J/m$^3$ with easy axis z. In order to test the validity of the methods from Sec. 3.3 for the Fe-Co-C material, these parameters were inserted into equation Eq. (6) and used in Eq. (5) to solve it using the Newton method. A comparison of these results to the results of the experiments is shown in Fig. 9. It turns out that Eq. (6), only in the ultra thin limit conforms to Eq. (5). For larger thicknesses, the approach of a root dependence is a better solution of Eq. (5). However, Eq. (6) seems to be the most compatible description with the experiment. Nevertheless, it is evident that the experimental results cannot be ideally described by any of the tested methods. In particular, none of them describes the transition of stripe domains to in-plane magnetization at a specific thickness. For this reason numerical micromagnetism is further used to investigate the stripe domains in Fe-Co-C.

## 5.1 Simulations

In order to investigate the Fe-Co-C material and in particular the property of stripe domains in-depth, simulations were performed with the simulation software magnum.fd [10]. This software is based on the theory of finite differences and has a built-in energy minimizer as well as a time integrator using LLG. For the first step the software is used to determine the single domain size of the Fe-Co-C material. Therefore small cubes with dimensions in the range of some multiples of the exchange length are simulated and relaxed with in-plane start magnetization, and with the consideration of exchange field, anisotropy field and the demagnetization field. As expected depending on the dimension of the cube, the system relaxed into three different states. A graphical representation of the magnetization of these states is shown in Fig. 2. The numerical calculations reveal a $l_\mathrm{SD}$ of $9.97\Delta_\mathrm{d}$. With a $Q = 0.228$ for Fe-Co-C this $l_\mathrm{SD}$ value seems to agree well with values for other materials found in literature. In



Die approbierte gedruckte Originalversion dieser Diplomarbeit ist an der TU Wien Bibliothek verfügbar
The approved original version of this thesis is available in print at TU Wien Bibliothek.
TU Bibliothek Your knowledge hub WIEN

Die approbierte gedruckte Originalversion dieser Diplomarbeit ist an der TU Wien Bibliothek verfügbar
The approved original version of this thesis is available in print at TU Wien Bibliothek.

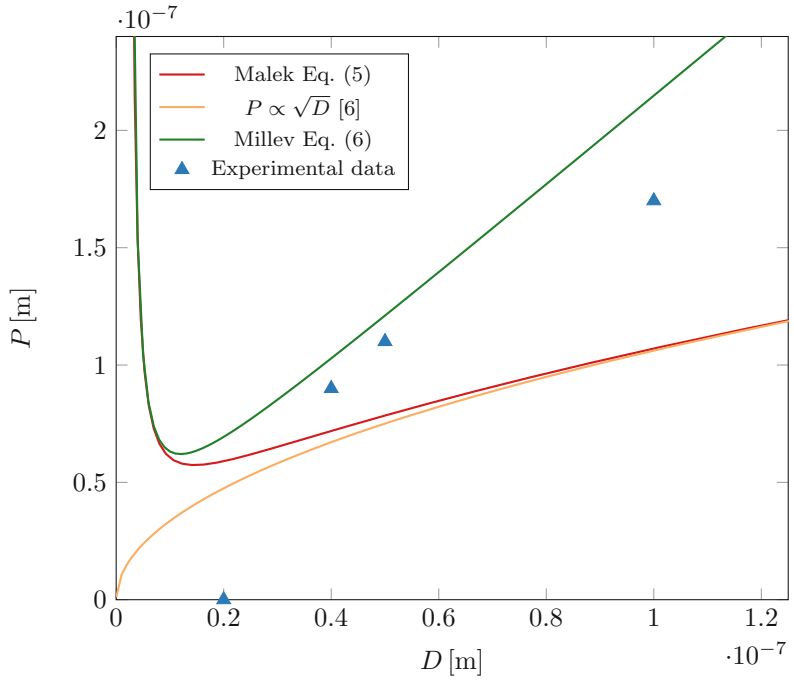


Figure 9: The plot shows a comparison of experimentally determined stripe period values with analytic methods. The red line is the nummerical solution of Eq. (5), the green line is calculated with Eq. (6) and the orange line is using an equation with a square root dependency of $P$ and $D$ [6]. The experimental data is represented with blue triangles.

contrast to structures with dimensions of only a few multiples of $\Delta_\mathrm{d}$, the following simulations cover thin extended films in which the mentioned stripes are found.

## 5.2 Multiple period simulations

Experiments have shown that in thin Fe-Co-C layers with a thickness in the two to three-digit nanometer range, the magnetization shows narrow stripe domains as described in Sec. 3.2. For the numerical analysis of this material and its stripe domains simulations according to the method described in 4.2.1 are performed. The simulated sample has a dimension of 4200 nm $\times$ 50 nm $\times$ $d$ with a cell size of 5 nm $\times$ 10 nm $\times$ 1 nm and periodic boundary conditions in the direction of the y-axis. The material parameters are $M_\mathrm{s} = 2.1/\mu_0$ T, $A = 28 \times 10^{-12}$ J/m and $K_1 = 0.4 \times 10^6$ J/m$^3$ with easy axis in z-direction. As predicted the magnetization configuration builds periodic waves as shown in Fig. 10. The calculation of the stripe periods confirms the behavior of an increasing period length with increasing thickness. However, the absolute values were below those predicted by the experiment. An undesirable side effect is that the periods are dependent on the x length. Due to the fact that the magnetization of this structure always forms an integer number of waves, the waves can be compressed or stretched compared to the minimum energy configuration in an infinite sample. This effect becomes smaller as the length of the structure increases, which, however, also means higher computational effort. Furthermore, it has been shown that the period length can be influenced by the starting magnetization by forcing a sine wave magnetization contribution with a certain wavelength before relaxing the system. This leads to the conclusion that, depending on the start configuration, the system relaxes into several energy minima which represent different stripe periods. For this reason, and since the periods simulated from an in-plane starting configuration are discovered to be quantitatively smaller than in the experiment, a new way of simulating the structure and calculating the period has been developed.

## 5.3 One period micromagnetics

For the reasons mentioned above, the same structure is further investigated with the one period micromagnetics method. The exact setup for these simulations is a cubic mesh with a cell size of 16 nm $\times$ 1 nm in the y- and z-axis directions. An example of a relaxed Fe-Co-C structure is given in Fig. 11, where the color coding



Die approbierte gedruckte Originalversion dieser Diplomarbeit ist an der TU Wien Bibliothek verfügbar
The approved original version of this thesis is available in print at TU Wien Bibliothek.
TU Bibliothek Your knowledge hub WIEN

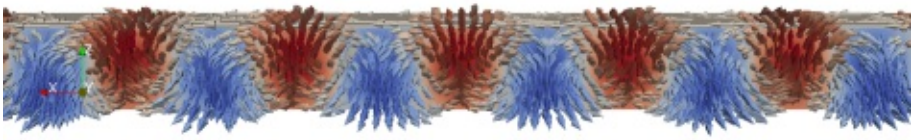

Figure 10: Magnetization distribution of a Fe-Co-C sample with $K_1 = 0.4$ MJ/m$^3$ and dimensions of 4200 nm $\times$ 50 nm $\times$ 50 nm with periodic boundary conditions in the y direction.

indicates the direction of the magnetization perpendicular component. The energy versus $L_x$ images, generated with this method, show a clearly recognizable minimum (e.g. Fig. 12).

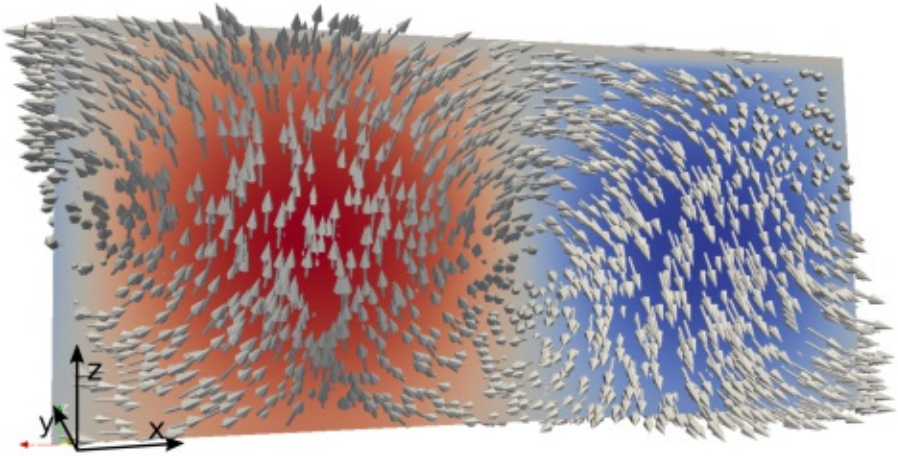


Figure 11: Relaxed Structure with a thickness of 50 nm and a $L_x$ of 113 nm. The red area is indicating a positive and the blue area a negative $m_z$, while the white arrows symbolize the magnetization vector.



Die approbierte gedruckte Originalversion dieser Diplomarbeit ist an der TU Wien Bibliothek verfügbar
The approved original version of this thesis is available in print at TU Wien Bibliothek.
TU Bibliothek Your knowledge hub WIEN

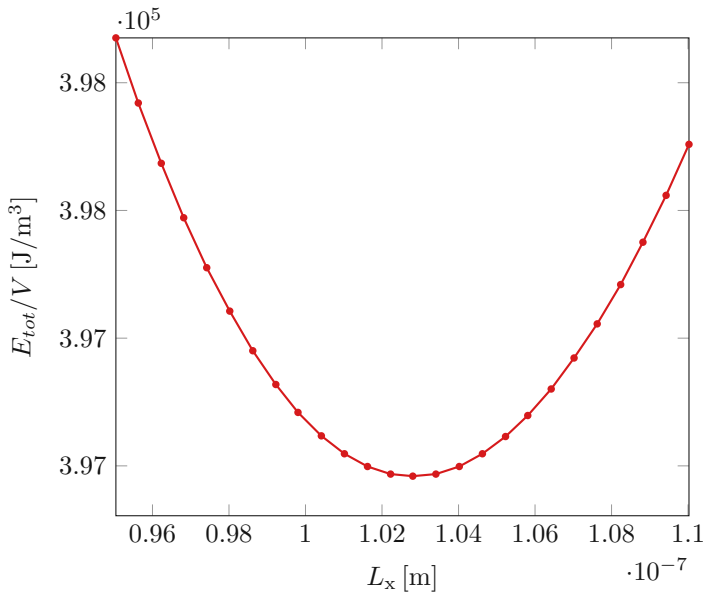


Figure 12: Energy density versus $L_x$ for a structure with a single wave period in the magnetization distribution. Therefore the length $L_x$ with the minimal energy indicates the optimal wavelength. The material parameters are $M_s = 2.1/\mu_0$T, $K_1 = 0.4$ MJ/m$^3$, $A = 28$ pJ/m and the thickness is $D = 45$ nm.

As mentioned above the start configuration of each step is taken from the result of the previous one. This procedure prevents a situation where the Energy versus $L_x$ plot shows an additional local minimum as shown in Fig. 13. It occurs if the stating $m_z$ is set to $\pm$ 0.5 for every step. In these local minima, $m_y$ changes its sign within the vortices and the magnetization turns inside, resulting in a higher energy distribution (Fig 14). Strictly speaking, this configuration lowers the anisotropy energy but increases the total energy. So, if the magnetization distribution of the first step is already close to the lower minimum, the method of sequential steps is preferable.



Die approbierte gedruckte Originalversion dieser Diplomarbeit ist an der TU Wien Bibliothek verfügbar
The approved original version of this thesis is available in print at TU Wien Bibliothek.
TU Bibliothek Your knowledge hub WIEN

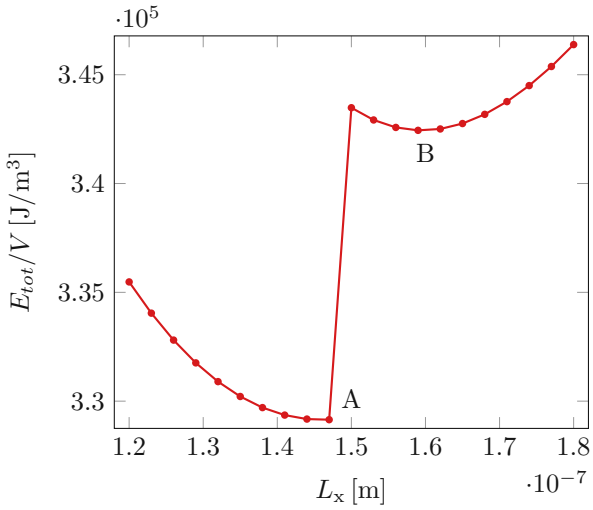


Figure 13: Energy density versus $L_x$ plot for a structure with $D = 70$ nm. An additional minimum occurs with slightly different configuration. A visualization of the magnetization distribution of the minima A can be seen in Fig. 11 and for the minima B in Fig. 14.

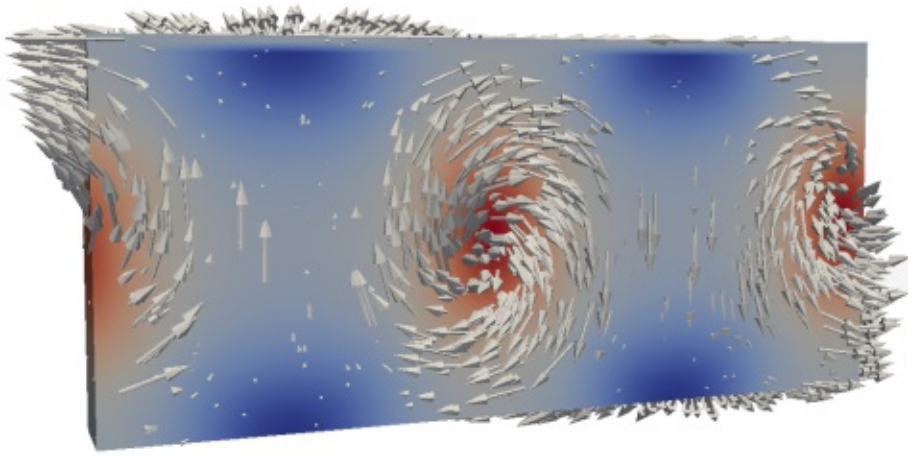

Figure 14: With a generic $m_z = \pm\ 0.5$ configuration as the starting point for each step, the magnetization within a vortex may point inward for some $L_x$. The blue and red colors are indicating a positive and negative $m_y$.

Simulations for thicknesses in the range of 45 nm to 130 nm show period lengths in good agreement with the experiment. A comparison of the simulated and the experimental



Die approbierte gedruckte Originalversion dieser Diplomarbeit ist an der TU Wien Bibliothek verfügbar
The approved original version of this thesis is available in print at TU Wien Bibliothek.
TU Bibliothek Your knowledge hub WIEN

data is given in Fig. 15. Figure 16 shows the simulated stray field amplitude 1 nm above the film for different thicknesses.

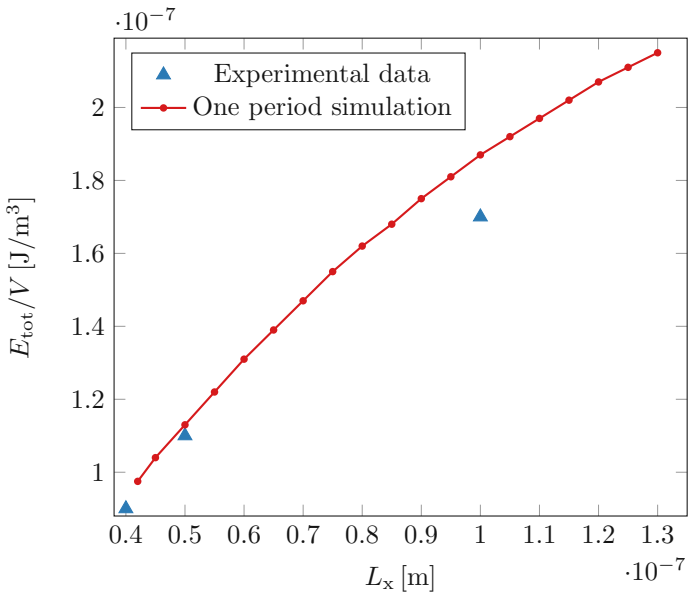


Figure 15: Stripe period versus the film thickness for a thin Fe-Co-C film. The red dots represent the calculated values using one period micromagnetic simulations with an anisotropy value of $K_1 = 0.4$ MJ/m$^3$ while the blue triangles are indicating the experimental data [1].

The results of this gradual method is then used to test the method of a rod-like cuboid elongated along the x-axis with periodic boundary condition in the direction of the y-axis. The relaxed structures with the optimal $\mathrm{L_x}$ are multiplied and lined up to form a structure with finite expansion along the x-axis. With this configuration as a starting point for a time integration the periods of the relaxed structures are close to the values of the gradually approach. This insight shows that the structure of finite expansion has more than one local minima and that is why previous simulations with in-plane starting magnetization showed different periods.

### 5.3.1 Validation of the simulation method

The purpose of this chapter is to confirm the functionality of the one period simulation method. Therefore, simulations were performed on structures with material parameters for which values for the $P(D)$ dependency already exist in the literature.



Die approbierte gedruckte Originalversion dieser Diplomarbeit ist an der TU Wien Bibliothek verfügbar
The approved original version of this thesis is available in print at TU Wien Bibliothek.
TU Bibliothek Your knowledge hub WIEN

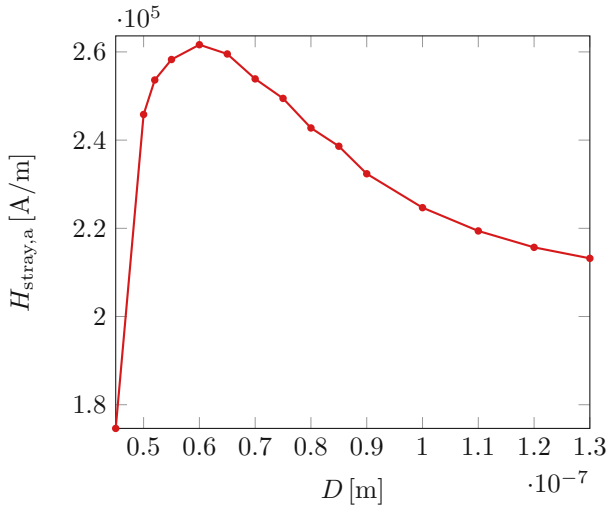


Figure 16: Amplitude $H_{\text{stray,a}}$ of the stray field 1 nm above the Fe-Co-C film versus the film thickness. The calculations are performed with a one period micromagnetic simulation method.

The method was used on cobalt films with two different parameter sets to compare the results with other simulations, experimental data and predictions from domain theory [7] [26]. The other simulated material was a Co-Pt film which also allowed a comparison to experimental data [6].

**Co Structure**

In literature both an experimental research and micromagnetic simulations for the description of thin cobalt films can be found. As in Fe-Co-C films, the experimentally observed stripes run roughly parallel on a length scale of some micrometers. The experimental and numerical analysis from individual research groups are assuming slightly different parameters for the saturation magnetization as well as the anisotropy and the exchange constant. Therefore two sets of simulations are performed to reconstruct their observations. In the first set of simulations, the material parameters $M_\text{s} = 1.78/\mu_0$ T, $K_1 = 0.46$ MJ/m$^3$ and $A = 13 \times 10^{-12}$ J/m are used according to Kisielewski et al. [26]. The result of these simulations can be seen in Fig. 17. The calculations of Kisielewski showed that the width increased with the square root of the thickness. That is why the results of the one period simulations are also fitted with a root function. The comparison of the resulting periods for the two simulation



Die approbierte gedruckte Originalversion dieser Diplomarbeit ist an der TU Wien Bibliothek verfügbar
The approved original version of this thesis is available in print at TU Wien Bibliothek.
TU Bibliothek Your knowledge hub WIEN

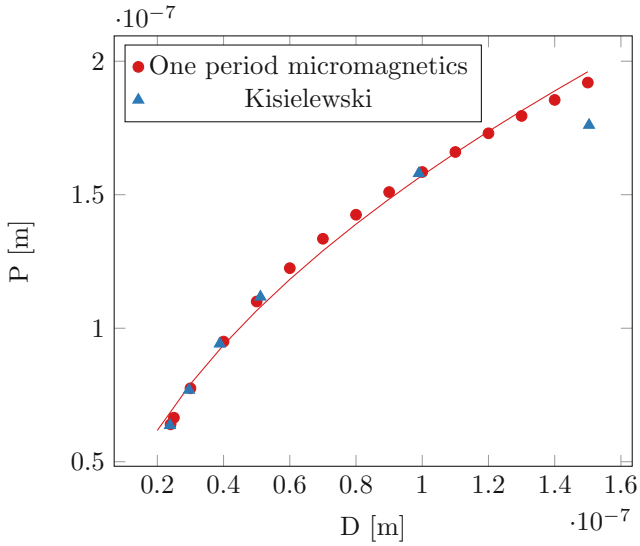


Figure 17: Comparison of stripe period calculations with a rod-shaped simulation structure of a few micrometers in length and PBC in the direction of the y axis (blue triangles) [26] and a one period micromagnetic simulation method for a cobalt film (red dots). The solid line represents a fit of the one period micromagnetic simulation data by the function $P(D) = c_1 * D^{1/2} + c_2$.

methods is less accurate for large thicknesses than for thinner films. Up to a thickness of 100 nanometers, the two simulation methods agree very well.

Additionally a comparison to experimental results is performed with material parameters of $M_s = 1.84/\mu_0$ T, $K_1 = 0.45$ MJ/m$^3$ and $A = 28 \times 10^{-12}$ J/m according to [7]. Figure: 18 extends the plot in Fig. 5 with the data from the one period simulation method. It is clearly recognizable that the simulated values allow a much better description of the experimental data than the analytical model. Also the collapse of the stripe domains below a critical thickness is consistent.

### Co-Pt Structure

The next set of simulations are made on the basis of a paper by M. Ghidini on Co-rich Co-Pt films with perpendicular anisotropy [6]. The group has experimentally and computationally investigated stripe domains in these films. The examined thicknesses go up to a size of one micrometer. Figure 19 shows the curve of the period over the layer thickness for experimentally determined and for calculated values. The calculations



Die approbierte gedruckte Originalversion dieser Diplomarbeit ist an der TU Wien Bibliothek verfügbar
The approved original version of this thesis is available in print at TU Wien Bibliothek.
TU Bibliothek Your knowledge hub WIEN

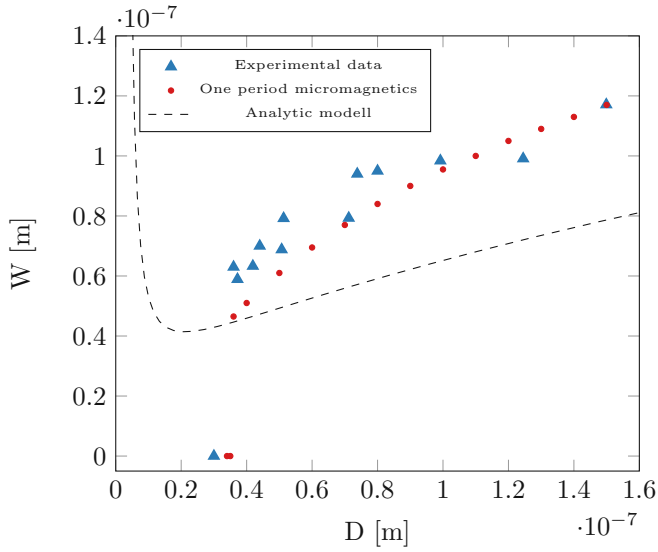


Figure 18: Experimentally observed domain width of thin cobalt films in comparison to the simulation. The blue triangles represent experimental results of Brandenburg [7] and Hehn [27]. The red dots show the results of the one period micromagnetic method. The dotted line represents calculations according to Malek and Kambersky [17] and are based on a modified Kittel model [14].

were determined with numerical micromagnetic calculations by [6] and with the one period micromagnetic method. Both simulations used the same material parameters of $M_s = 600$ kA/m, $A = 1.4 \times 10^{-11}$ J/m and $K_1 = 3.45 \times 10^5$ J/m$^3$. The graphical representation of the magnetization distribution of the one period micromagnetic simulation method (Fig. 20) and from calculations of M. Ghidini et al. (Fig. 21) show a similar image. Between domains with positive and domains with negative magnetization narrow vortices are formed. The domain itself is largely homogeneous. The width of the vortices indicating the domain wall width remain almost constant with varying thickness.



Die approbierte gedruckte Originalversion dieser Diplomarbeit ist an der TU Wien Bibliothek verfügbar
The approved original version of this thesis is available in print at TU Wien Bibliothek.
TU Bibliothek Your knowledge hub WIEN

Die approbierte gedruckte Originalversion dieser Diplomarbeit ist an der TU Wien Bibliothek verfügbar
The approved original version of this thesis is available in print at TU Wien Bibliothek.

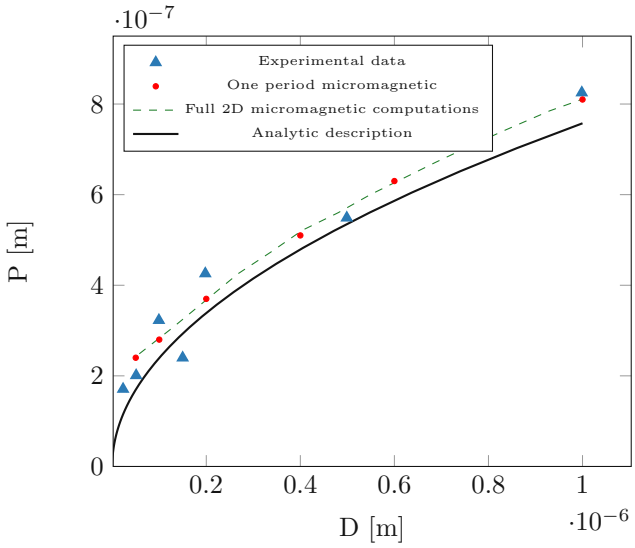


Figure 19: Period as a function of the film thickness for a thin Co-Pt layer. Experimentally determined values [6] obtained from MFM images are represented by blue triangles. The red dots are symbolizing the simulation results from the one period micromagnetic calculations while the green dotted line is representing calculations performed by Ghidini et al. [6]. The black line is an analytical description that assumes a square-rooted dependence of the period and the thickness, as postulated by Ghidini [6].

Die approbierte gedruckte Originalversion dieser Diplomarbeit ist an der TU Wien Bibliothek verfügbar
The approved original version of this thesis is available in print at TU Wien Bibliothek.

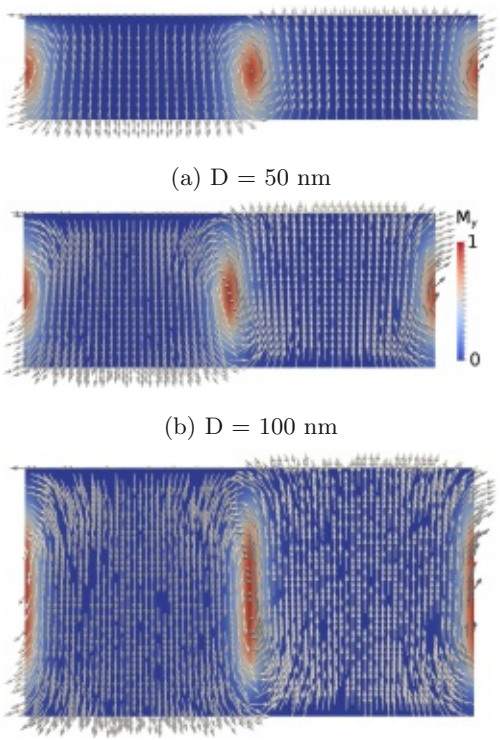


(a) D = 50 nm

(b) D = 100 nm

(c) D = 200 nm

Figure 20: Cross section view of the structure showing the magnetization distribution for some thicknesses. The coloring is indicating the magnitude of the magnetization component pointing inwards. The material parameters for this simulations of Co-Pt are $M_s = 600$ kA/m, $A = 1.4 \times 10^{-11}$ J/m and $K_1 = 3.45 \times 10^5$ J/m$^3$.

Die approbierte gedruckte Originalversion dieser Diplomarbeit ist an der TU Wien Bibliothek verfügbar
The approved original version of this thesis is available in print at TU Wien Bibliothek.

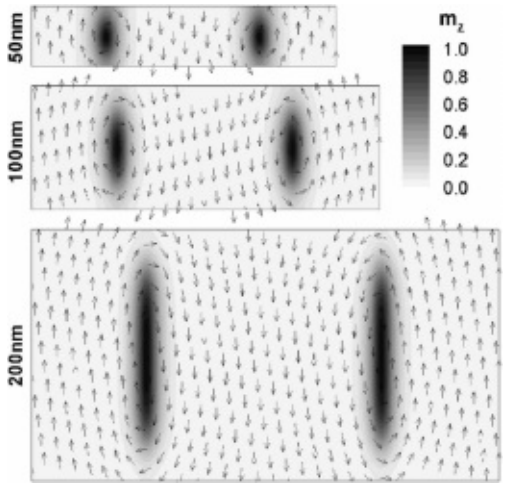


Figure 21: A cross section view of Co-Pt in analogy to Fig. 20 determined by M. Ghidini [6] with full 2D micromagnetic computations. The material parameters are identical to those used for Fig. 20.

## 5.4 Varying material parameters

Simulations have shown that the wavelength of the stripes depend on the anisotropy constant $K_1$. Figure 22 shows a plot of the period for some anisotropy constants near the value of $0.4 \times 10^6$ J/m$^3$ of Fe-Co-C. It appears that there is a critical thickness at which the period is independent of the anisotropy constant. Underneath this thickness the period increases with $K_1$ but decreases above that value. To describe this behavior a fit for $p(d, k)$ has been made. As a fit function,

$$p(d,k) = 1.467 \times 10^{-07} \left( \frac{d + c_0}{c_1} \right)^{\frac{c_2}{k+c_3}} \tag{24}$$

was chosen, where 1.467 is the value of the period at the critical thickness and $c_{0-4}$ are the fit parameters. The property of functions with different fractional exponents to intersect at a single point was used to describe the simulation results. The calculated fit parameters are $c_0 = -0.199 \pm 0.0067$, $c_1 = 0.503 \pm 0.0074$, $c_2 = 49.213 \pm 1.7678$, $c_3 = 55.599 \pm 3.3004$. A percentage error of the fit is calculated with:

$$F = \frac{1}{N} \sum\nolimits_{n=0}^{N} \frac{(p_\mathrm{n} - p_\mathrm{fit,n})}{p_\mathrm{n}}, \tag{25}$$

where N is the number of points, $p_\mathrm{n}$ are the simulated period values and $p_\mathrm{fit,n}$ are the corresponding fitted values. The fit function Eq. (24) gives an error of $F = 0.62\%$. For comparison Fig. 22 is also plotted with a different fit function (Eq. (26)) which furnishes a bigger error of $F = 0.92\%$.

$$p(d,k) = K_1 c_0 + \frac{(d - 0.7)(c_1 - K_1)c_2}{\sqrt{d}} + c_3 \tag{26}$$

For visibility reasons Fig. 23 shows the optimal fit with Eqn. (24) for only a few different $K_1$ values.



Die approbierte gedruckte Originalversion dieser Diplomarbeit ist an der TU Wien Bibliothek verfügbar
The approved original version of this thesis is available in print at TU Wien Bibliothek.
TU Bibliothek Your knowledge hub WIEN

Die approbierte gedruckte Originalversion dieser Diplomarbeit ist an der TU Wien Bibliothek verfügbar
The approved original version of this thesis is available in print at TU Wien Bibliothek.

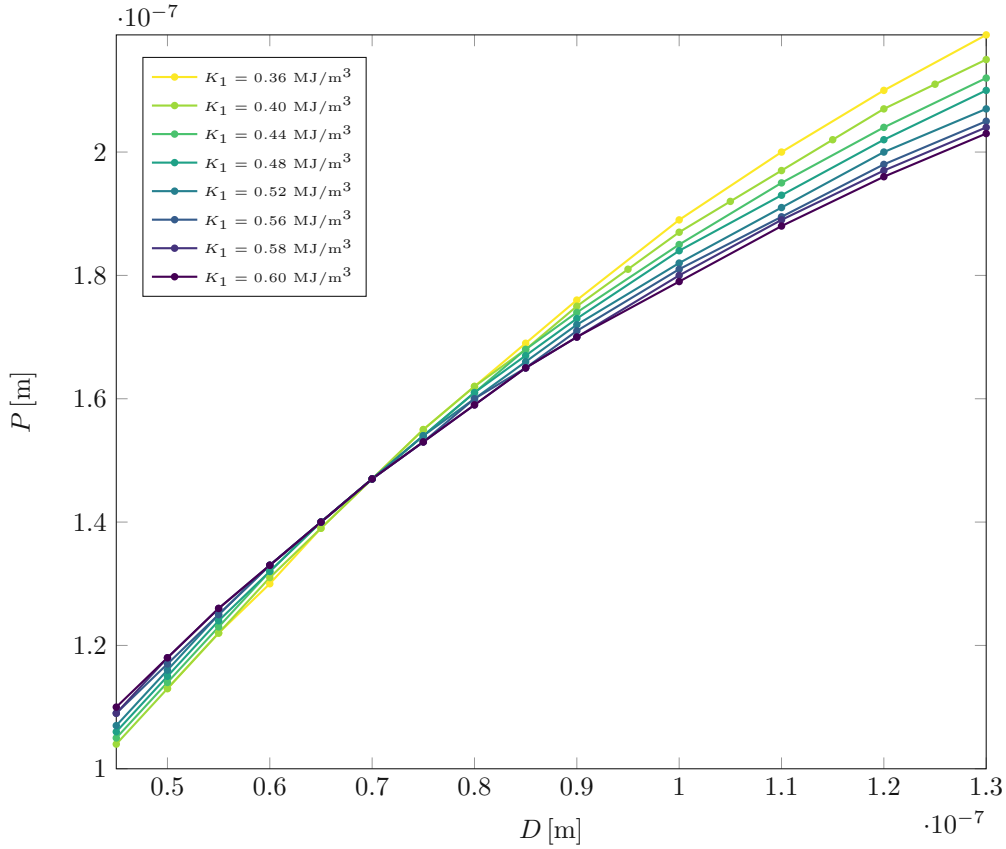


Figure 22: Stripe period versus thickness for some anisotropy constants. The connecting lines are added to guide the eye.

Die approbierte gedruckte Originalversion dieser Diplomarbeit ist an der TU Wien Bibliothek verfügbar
The approved original version of this thesis is available in print at TU Wien Bibliothek.

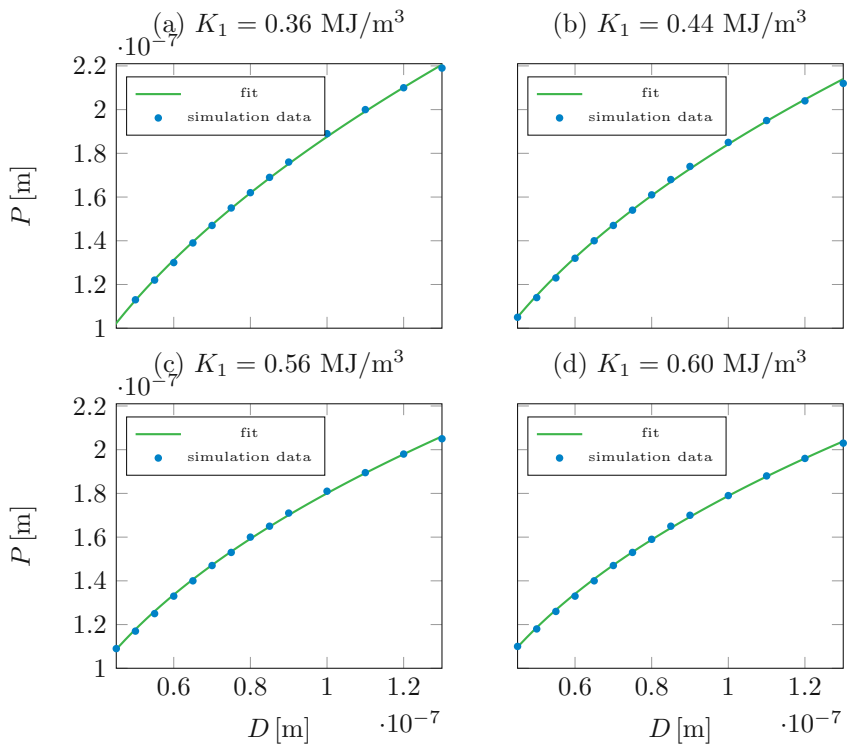


Figure 23: Fitted period versus thickness plot for some $K_1$. All shown fit curves are created with identical fit parameters.

In addition to the influence of the anisotropy constant on the wavelength also the dependency of the exchange constant is examined. As the simulations show, the period increases as the exchange constant increases (Fig. 24). This behavior is predictable, since a high $A$ increases the energy of the domain walls and therefore . Since the experimental data comes in the form of MFM images taken from the stray field just above the sample, it is important to also determine the influence of $K_1$ and $A$ on the strength of this field. Therefore the stray field is evaluated one nanometer above the Fe-Co-C structure. To check if the distance to the structure has an impact on the amplitude $H_{\text{stray,a}}$, the discretization in direction of the z-axis is scaled down. Doing so allows, to calculate $\boldsymbol{H}_{\text{stray}}$ at a closer distance above the structure. These simulations show that a smaller discretization just allows a finer calculation of $\boldsymbol{H}_{\text{stray}}$, but has no quantitative impact. Similar to the wavelength, $\boldsymbol{H}_{\text{stray}}$ is also strongly dependent on the anisotropy constant but does not change much with the exchange constant. As one can see in Fig 25a the amplitude of $\boldsymbol{H}_{\text{stray}}$ more than doubles with a $K_1$ in the range from 0.36 to 0.68 MJ/m$^3$. In contrary the exchange constant has a smaller impact on $\boldsymbol{H}_{\text{stray}}$. Figure 26 gives a more comprehensive look on the behavior of $\boldsymbol{H}_{\text{stray}}$ for different anisotropy and exchange constants by plotting the amplitude. The stray field amplitude has a maximum for an exchange constant in the range of $20 \times 10^{-12}$ J/m.



Die approbierte gedruckte Originalversion dieser Diplomarbeit ist an der TU Wien Bibliothek verfügbar
The approved original version of this thesis is available in print at TU Wien Bibliothek.
TU Bibliothek Your knowledge hub WIEN

Die approbierte gedruckte Originalversion dieser Diplomarbeit ist an der TU Wien Bibliothek verfügbar
The approved original version of this thesis is available in print at TU Wien Bibliothek.

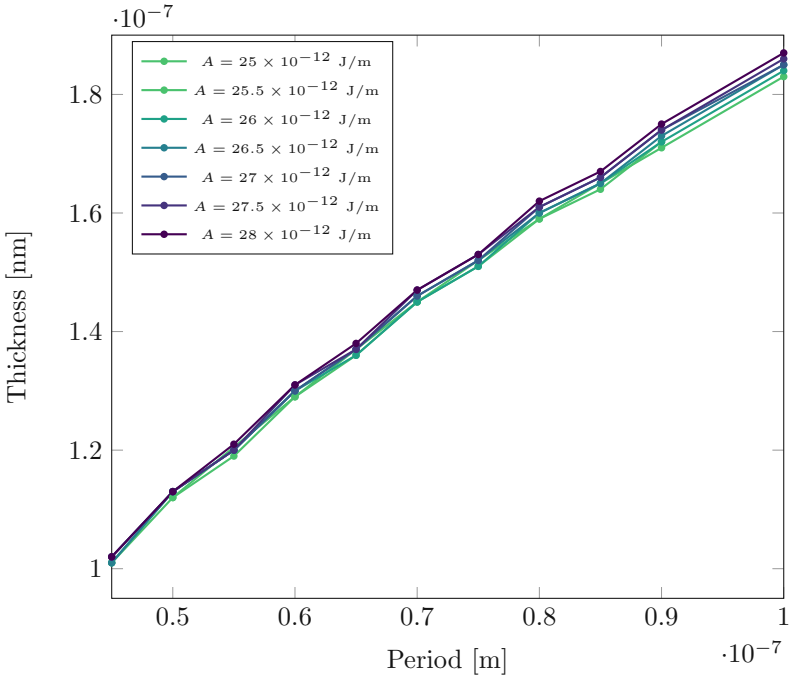


Figure 24: Stripe period versus thickness for some exchange constants.

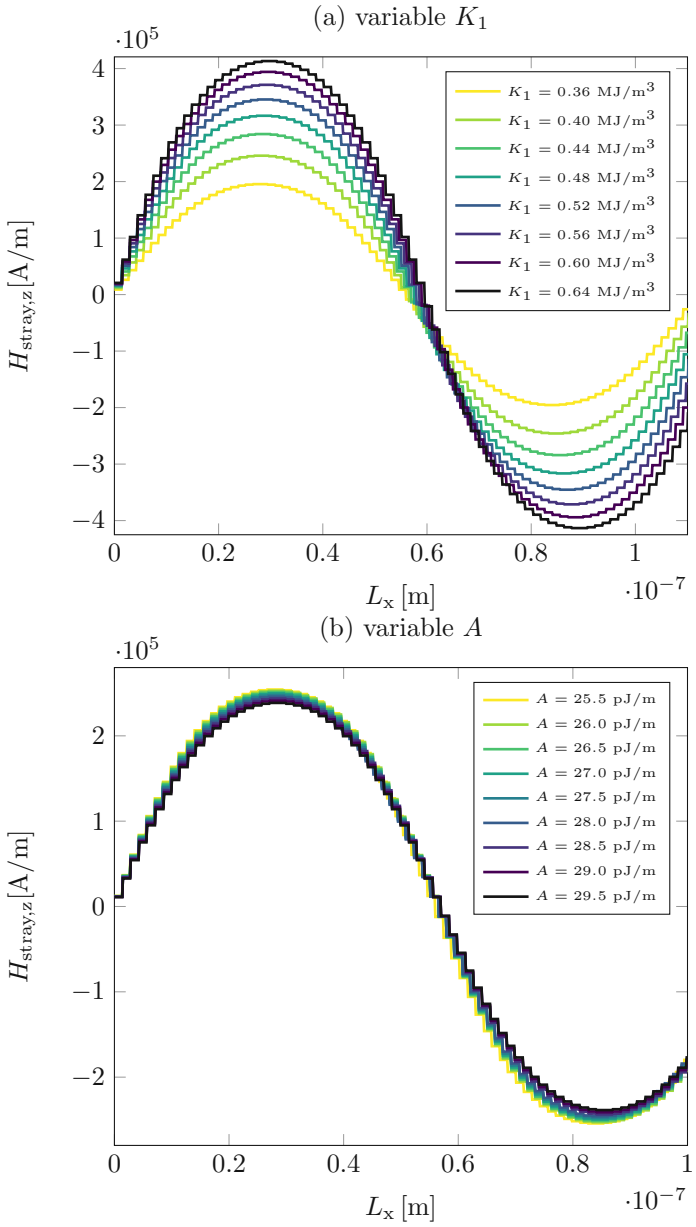


Figure 25: The stray field z component $H_{\text{stray,z}}$ measured 1 nm above a 50 nm thick structure.



Die approbierte gedruckte Originalversion dieser Diplomarbeit ist an der TU Wien Bibliothek verfügbar
The approved original version of this thesis is available in print at TU Wien Bibliothek.
TU Bibliothek Your knowledge hub WIEN

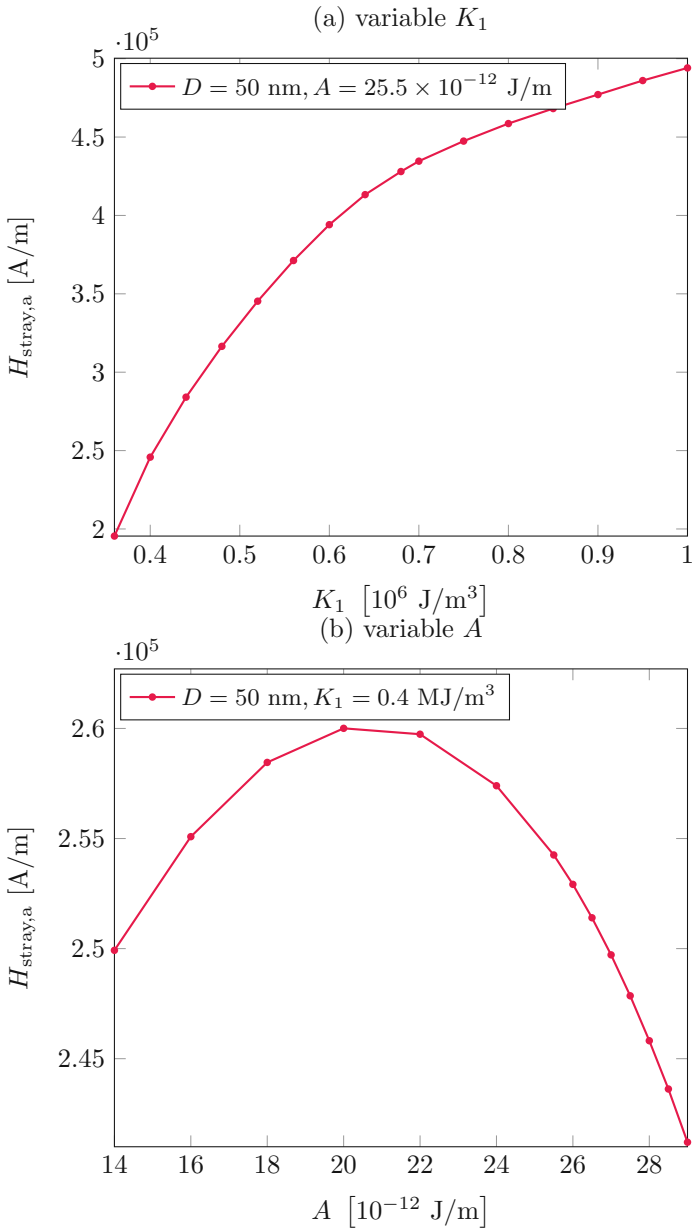


Figure 26: Stray field amplitude versus anisotropy or exchange constant for a structure with a thickness of 50 nm.



Die approbierte gedruckte Originalversion dieser Diplomarbeit ist an der TU Wien Bibliothek verfügbar
The approved original version of this thesis is available in print at TU Wien Bibliothek.
TU Bibliothek Your knowledge hub WIEN

## 5.5 Minimal thickness for the formation of stripe patterns

Not only the period, but also the minimum thickness at which the magnetization still forms stripe domains depends on the anisotropy constant. This section describes the analysis of the structure with a thickness in the range of this minimum thickness. In order to obtain information on the behavior of the magnetization in this critical regime, simulations are performed with a high range of $\mathrm{L_x}$ for some different $K_1$ values. The simulations of each structure of different anisotropy constant show the same behavior when $D$ is gradually increased up to the minimal thickness. Just below the minimum thickness the magnetization distribution is in-plane. While increasing $D$, a specific thickness for each $K_1$ can be found, where the magnetization relaxes in two different kind of states as can be seen in Fig. 28a,b. A plot for the energy density as a function of the length $L_\mathrm{x}$ for this thickness (Fig. 27a) shows multiple minima separated by a section of constant energy density. These minima indicate a configuration with strong stripe domains, as observed in the experiment. The first minimum indicates a magnetization with only one period and therefore gives us the critical wavelength for the critical thickness for this specific $K_1$. The second minimum results from the fact that as $L_\mathrm{x}$ increases, a configuration with more than one period becomes energetically more favourable. The individual minima therefore indicate the same wavelength (Fig. 28a,c). In the case of Fig. 27a, where the thickness is very close to the critical thickness, the minimum for a magnetization with exactly two periods does not occur and the magnetization is in-plane instead. This section of an in-plane magnetization becomes smaller at greater thicknesses, and a new minimum with two periods appears (Fig. 27b). The simulations show that the critical thickness decreases with increasing $K_1$ (Fig. 29), which means that for materials with high anisotropy, stripe domains appear in even thinner layers. The results of the critical values for simulations with $K_1 = 0.4$ MJ/m$^3$ are $D_\mathrm{crit} = 42$ nm and $W_\mathrm{crit} = 47.5$ nm for the critical stripe width. They correspond remarkably well with the predictions for a $Q = 0.228$ in Sec. 4.1.1 (red dot in Fig. 7 and 8).



Die approbierte gedruckte Originalversion dieser Diplomarbeit ist an der TU Wien Bibliothek verfügbar
The approved original version of this thesis is available in print at TU Wien Bibliothek.
TU Bibliothek Your knowledge hub WIEN

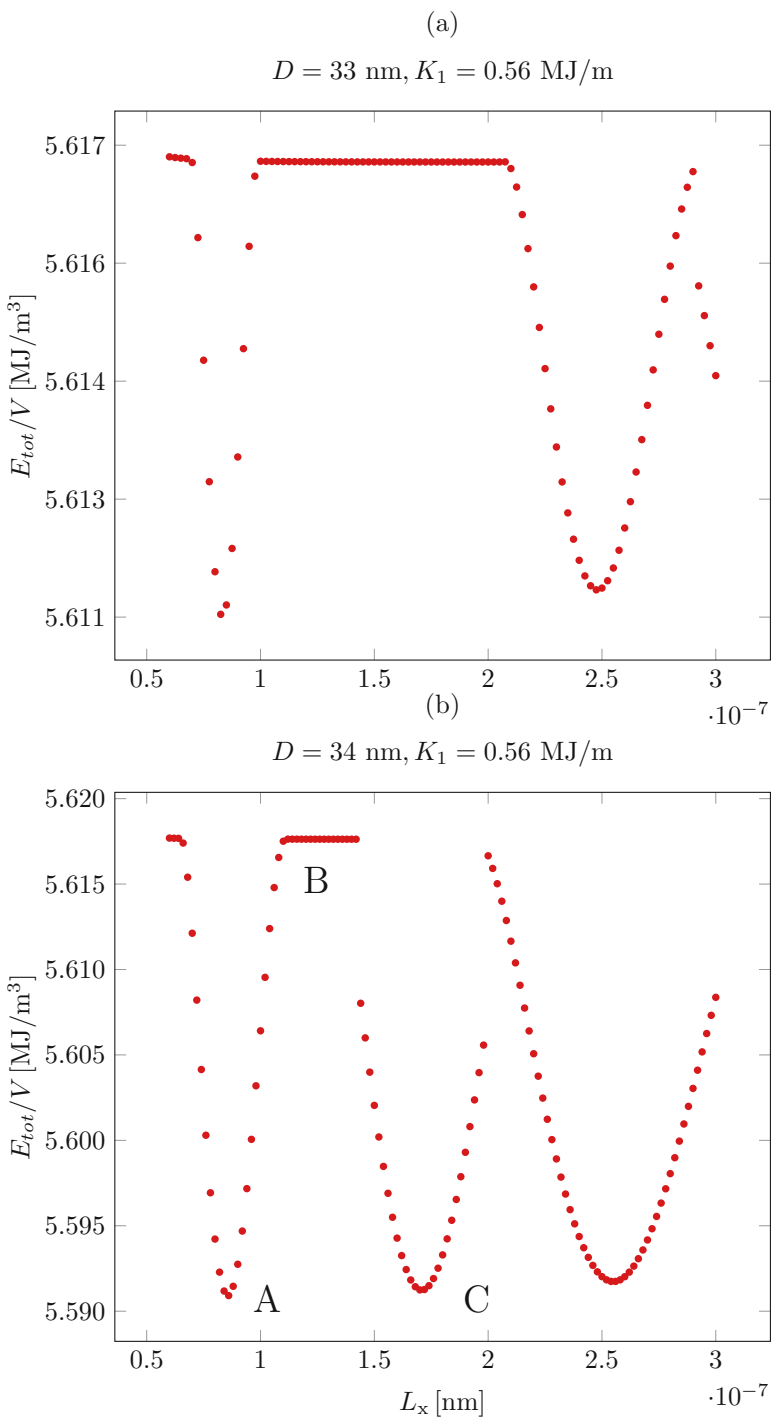


Figure 27: Enegy density vs. $L_x$ plot for a structure with $K_1 = 0.56 \times 10^6$ J/m$^3$, $A = 28 \times 10^{-12}$ J/m and $M_s = 2.1/\mu_0$ T. (a) The stripe domains first appear at a thickness of $D = 33$ nm. The parabola at $L_x = 83$ nm indicates the formation of a single wave period in the magnetization, while in the region around $L_x = 249$ nm the magnetization forms three periods. The magnetization is in-plane in the region of constant energy density. (b) At $D = 34$ nm the plot additionally shows a section where the magnetization has two periods. A visualization of the magnetization distribution at the points A, B and C can be seen in Fig. 28 a,b and c respectively.

Die approbierte gedruckte Originalversion dieser Diplomarbeit ist an der TU Wien Bibliothek verfügbar
The approved original version of this thesis is available in print at TU Wien Bibliothek.
TU Bibliothek Your knowledge hub WIEN

Die approbierte gedruckte Originalversion dieser Diplomarbeit ist an der TU Wien Bibliothek verfügbar
The approved original version of this thesis is available in print at TU Wien Bibliothek.

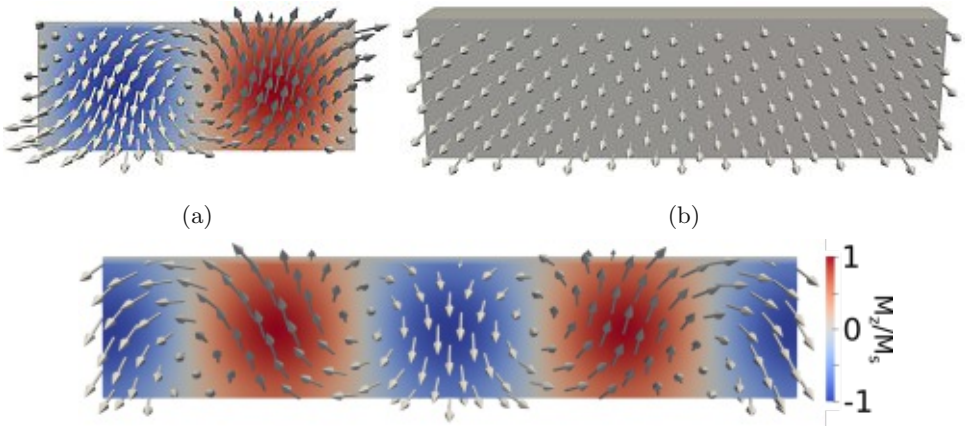


(c)

Figure 28: Cross section view of a structure with $K_1 = 0.56 \times 10^6$ J/m$^3$, $A = 28 \times 10^{-12}$ J/m and $M_s = 2.1/\mu_0$ T. The thickness is 34 nm which is 1 nm above the critical thickness. The three structures differ only in length. This results in the different magnetization distributions. (a), (b) and (c) show the magnetization at the points A, B and C of Fig. 27b. Structure (a) has a length of 86 nm and a single period in the magnetization. (b) has a length of 126 nm and in-plane magnetization. (c) has a length of 172 nm where the magnetization forms two whole periods. The color coding is visualizing the magnetizations z component.

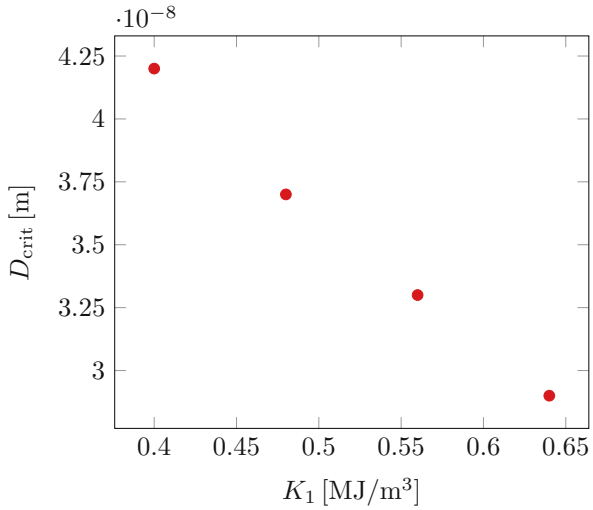


Figure 29: Change of the critical thickness with increasing $K_1$.

## 5.6 Analysis of experimental stray field data

This chapter covers the analysis of the experimental stray field data. To experimentally determine the quantitative values of the stray field at the surface of the sample, the surface charge $\sigma$ is measured with a magnetic force microscope. The stray field is then calculated with $H_{\text{stray,z}} = \sigma/2$ [1]. A comparison of the experimental stray field measurement and the data simulated with $K_1 = 0.4$ MJ/m$^3$ shows that the experimental values are significantly higher. Simulations have shown that an increase in the anisotropy constant results in a higher stray field magnitude, therefore a specific $K_1$ can be found for which the simulated and experimental $H_{\text{stray,z}}$ data match. The variation of $K_1$ shows a good agreement of the $\boldsymbol{H}_{\text{stray}}$ amplitude only at a $K_1$ value of 0.58 MJ/m$^3$ (Fig. 30). A $K_1$ of 0.58 MJ/m$^3$ represents an increase of almost 50% compared to the value assumed by [1]. Whether such an inaccuracy can be explained by the experimental determination of the anisotropy constant or whether an exact comparison of the stray field from simulations and experiments is not suitable cannot be clarified.

Another interesting observation when looking at the MFM images, is that both the amplitude and the period of the stray field are not constant across the film. For this reason, only a mean value of large distributed values can be taken as experimental stripe domain width for a specific film thickness. As an example, for a film thickness



Die approbierte gedruckte Originalversion dieser Diplomarbeit ist an der TU Wien Bibliothek verfügbar
The approved original version of this thesis is available in print at TU Wien Bibliothek.
TU Bibliothek Your knowledge hub WIEN

Die approbierte gedruckte Originalversion dieser Diplomarbeit ist an der TU Wien Bibliothek verfügbar
The approved original version of this thesis is available in print at TU Wien Bibliothek.

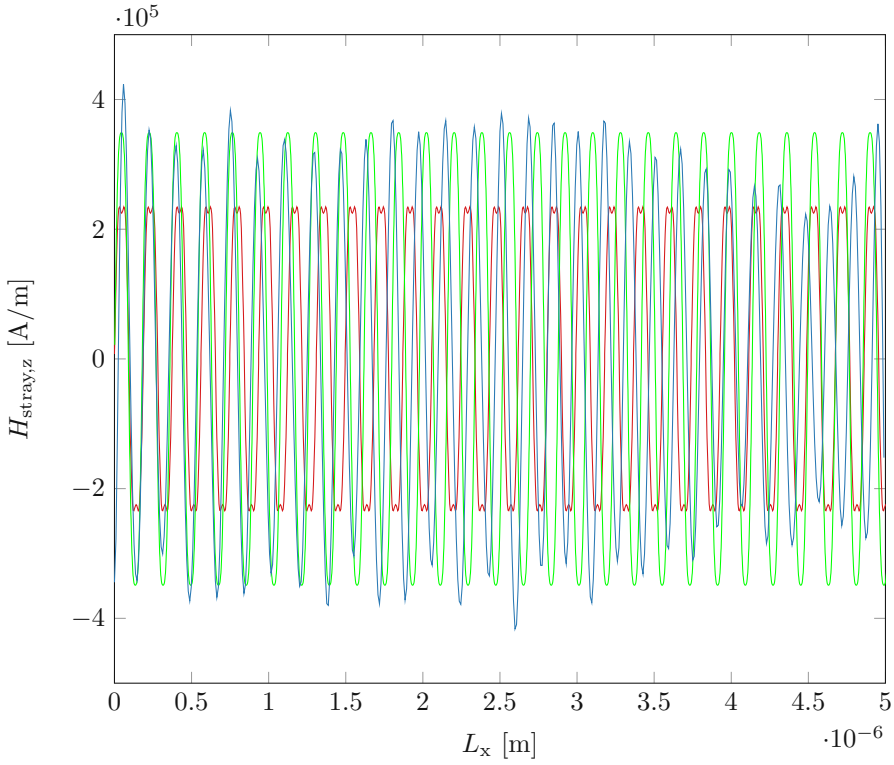


Figure 30: Stray field above a Fe-Co-C film with a thickness of 100 nm. The blue line is indicating the experimental data, while the red and green lines are the simulation results with $K_1 = 0.4$ MJ/m$^3$ and $K_1 = 0.58$ MJ/m$^3$ respectively.

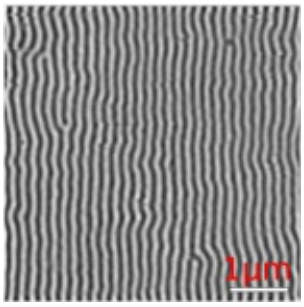


(a)

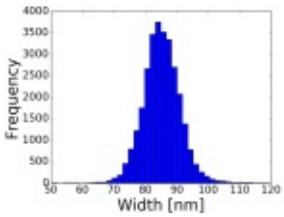


(b)

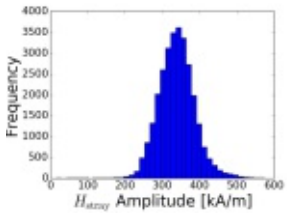


(c)

Figure 31: MFM image of a 100 nm thick Fe-Co-C sample (a). The period of the stripes as well as the amplitude of the strayfield above the surface is not constant. (b) and (c) show histograms of the distribution of the width and the amplitude of the stripes

of 100 nm periods of 140 nm to 200 nm occur (Fig. 31b). To find the reason for the strongly varying stray field amplitude, the parameters that influence the stray field are considered. Possible reasons are a potential direct dependence of amplitude and period, a non-constant film thickness, anisotropy constant or saturation magnetization. The first step is to determine if there is a dependence between the experimental stray field amplitude and stray field period and if so, what this dependence is. For this purpose, the area in Figure 31 is scanned and a plot of the individual amplitudes to the corresponding stripe thickness is created. This plot can be fitted with a linear fit function which reveals a positive slope of $H_{\mathrm{stray,a}}$ with the period (Fig. 32). Since the stripes are not exactly aligned in the same direction, a small inaccuracy in the calculated period length is to be expected.

A change in the saturation magnetization has shown that the period decreases with increasing $M_{\mathrm{s}}$. For this reason and because $H_{\mathrm{stray,a}}$ increases with $M_{\mathrm{s}}$, the monotonous increase of $H_{\mathrm{stray,a}}(P)$ cannot be attributed to a non-constant $M_{\mathrm{s}}$. The first assump-



Die approbierte gedruckte Originalversion dieser Diplomarbeit ist an der TU Wien Bibliothek verfügbar
The approved original version of this thesis is available in print at TU Wien Bibliothek.
TU Bibliothek Your knowledge hub WIEN

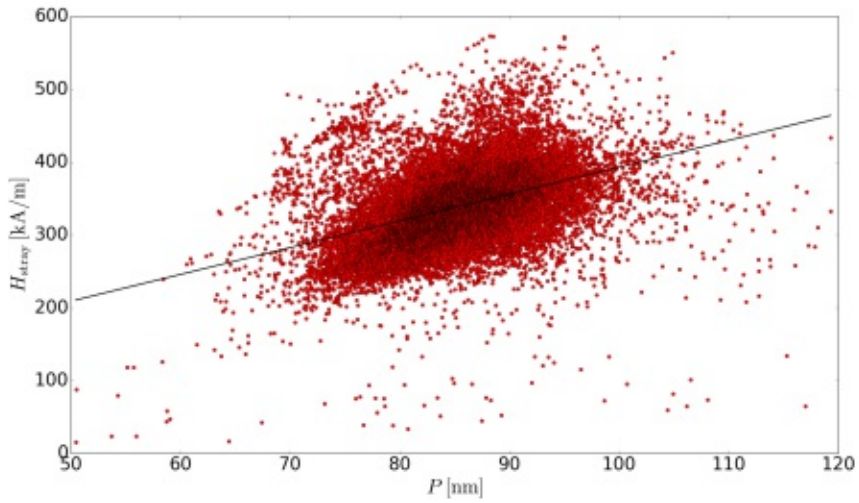


Figure 32: Dependence of the absolute values of the stray field amplitudes versus their corresponding stripe width over the 100 nm thick sample. The black line represents the best linear fit.

tion is that even with constant thickness and anisotropy constant, in the real medium different periods occur, which then directly influence the stray field. If this is the case, the simulated stray field should show the same dependency as in Fig. 32 for forced period changes at constant $D$ and $K_1$. The results of these simulations for two anisotropy constants and for $D = 100$ nm can be seen in Fig. 33. The stray field rapidly increases for periods smaller than 100 nm and slightly falls of afterwards. For $K_1 = 0.4$ MJ/m$^3$ and for periods greater than 160 nm the crests and valleys of the $\boldsymbol{H}_{\text{stray}}$ waveform show indentations, which is why the plot in Fig. 33 is divided into two branches representing the maximum and minimum of this indentation. This indentations, which can be seen in Fig. 30, cannot be observed in the MFM image and show again that the simulated field with higher $K_1$ matches the experiment better. It turns out that $H_{\text{stray,a}}$ actually decreases in the essential period range in contrast to the experiment, which leads to the assumption that the increase in Fig. 32 is caused by non-constant material parameters across the structure. To find out if this parameter is either one of the two, $K_1$ or $D$, $H_{\text{stray,a}}$-versus-$P$ plots were made, where the different periods were generated by varying one of the respective parameters. As can be seen in Fig. 34 the same $H_{\text{stray,a}}(P)$ dependence cannot be determined in either simulation type. In



Die approbierte gedruckte Originalversion dieser Diplomarbeit ist an der TU Wien Bibliothek verfügbar
The approved original version of this thesis is available in print at TU Wien Bibliothek.
TU Bibliothek Your knowledge hub WIEN

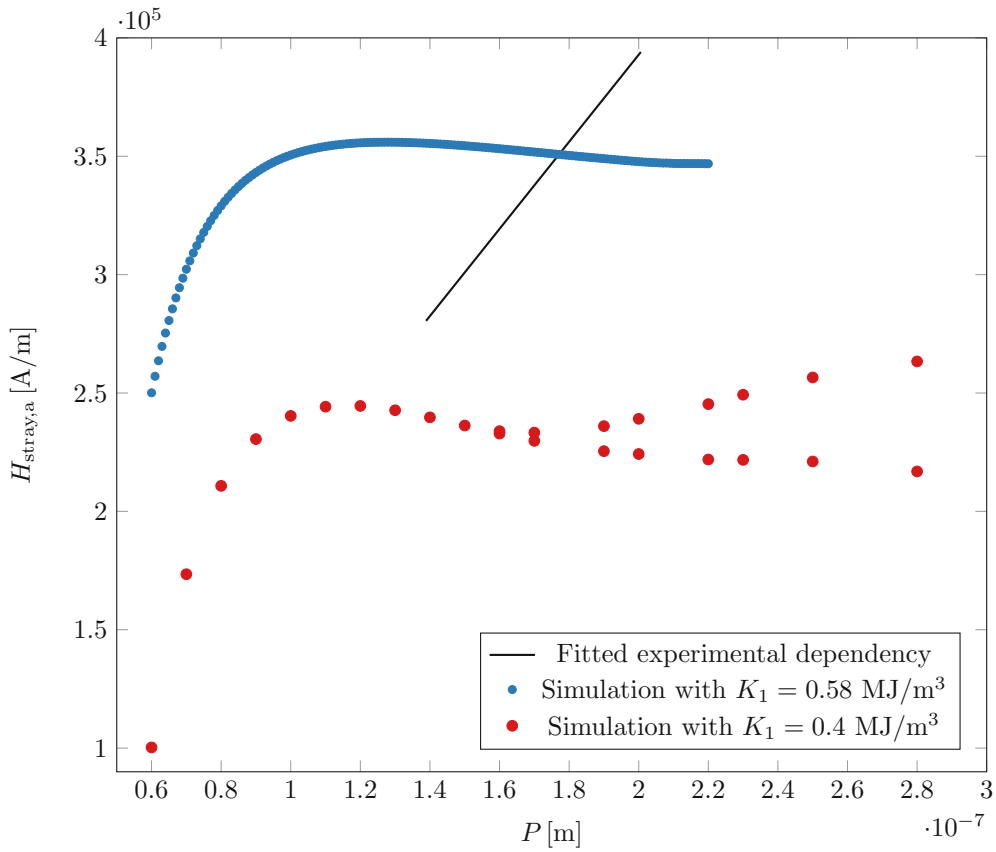


Figure 33: Stray field amplitude versus period plot for a fixed thickness of 100 nm and for two different anisotropy constants. Not only the period of the energy minimum, but also smaller and larger specified periods are displayed. The material parameters are kept constant. An indentation of the stray field wave at $K_1 = 0.4$ MJ/m$^3$ is the reason for the two branches of red dots. The black line is representing the best linear fit of the experimental data.

both cases $H_{\text{stray,a}}$ decreases instead of increasing with increasing period. Therefore the unstable behavior of $\boldsymbol{H}_{\text{stray}}$ cannot be attributed to these parameters.

## 5.7 Simulation of a finite structure

The experimental MFM images of the Fe-Co-C film show that the stripes are only locally parallel. The global view exposes three different domain walls. One is a 180 degrees flip (Fig. 36a) of the magnetization component in the direction of the stripes,



Die approbierte gedruckte Originalversion dieser Diplomarbeit ist an der TU Wien Bibliothek verfügbar
The approved original version of this thesis is available in print at TU Wien Bibliothek.
TU Bibliothek Your knowledge hub WIEN

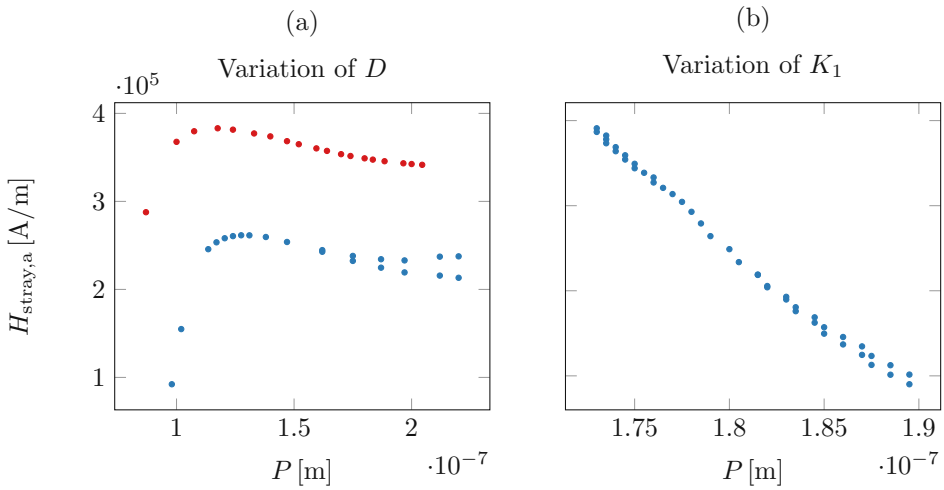


Figure 34: The plots show the change in $H_{\text{stray,a}}$ for different periods. In plot (a) the period is altered by varying the thickness. The red dots are generated with a constant $K_1$ of 0.58 MJ/m$^3$ and the blue dots with $K_1 = 0.4$ MJ/m$^3$. The anisotropy constant is varied in (b) while the thickness is kept constant at 100 nm.

indicated by the black arrows in Fig. 35. In Fig 11 this would be the y component. The second domain wall that appears in the MFM images is a 90° rotation of the direction of the stripes. Due to the demagnetization field, four of these 90° rotations can form a vortex structure (Fig. 36b,c).

These kinds of domain walls can also be reproduced in the simulations. Therefore, the relaxed structure from previous multiple period simulations of Sec. 5.2 are multiplied and arranged to form 90° and 180° domain walls. The 180° domain wall, shown in Fig. 37, could be identified as a Bloch-wall as the magnetization rotates out of the plane of the domain wall. Periodic boundary conditions in the direction of the y-axis could be used for this simulation. Figure 38 shows how the demagnetization field forces the magnetization to form a vortex structure if the simulation is started with two 90° rotations.



Die approbierte gedruckte Originalversion dieser Diplomarbeit ist an der TU Wien Bibliothek verfügbar
The approved original version of this thesis is available in print at TU Wien Bibliothek.
TU Bibliothek Your knowledge hub WIEN

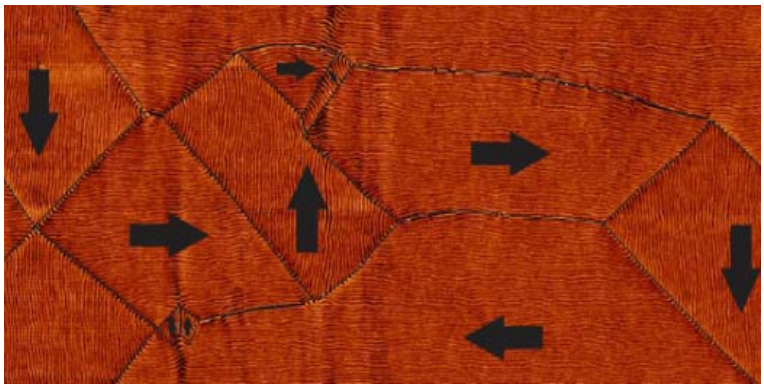

Figure 35: MFM Image of a Fe-Co-C thin film showing stripe domains in the magnetization distribution. [2]

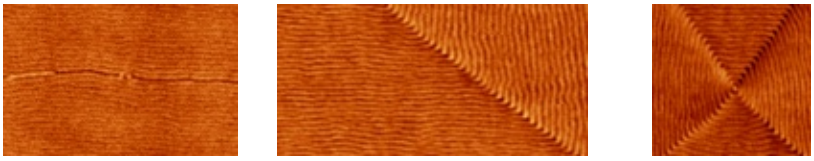

(a) (b) (c)

Figure 36: (a) 180˚, (b) 90˚ and (c) vortex domain wall

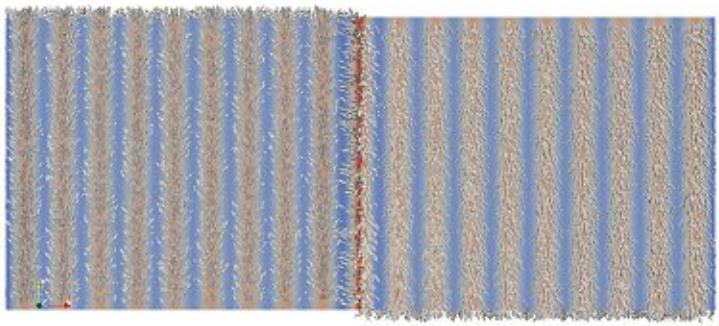

Figure 37: Bloch domain wall between an area with negative $m_y$ and positive $m_y$.



Die approbierte gedruckte Originalversion dieser Diplomarbeit ist an der TU Wien Bibliothek verfügbar
The approved original version of this thesis is available in print at TU Wien Bibliothek.
TU Bibliothek Your knowledge hub WIEN

Die approbierte gedruckte Originalversion dieser Diplomarbeit ist an der TU Wien Bibliothek verfügbar
The approved original version of this thesis is available in print at TU Wien Bibliothek.

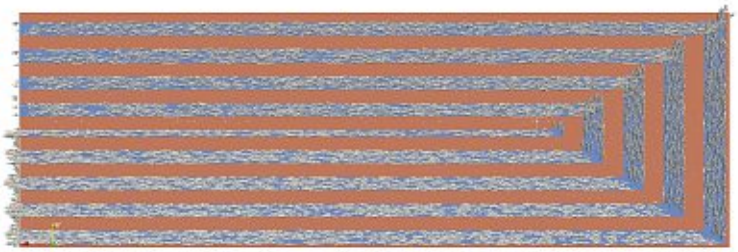

(a) Start configuration

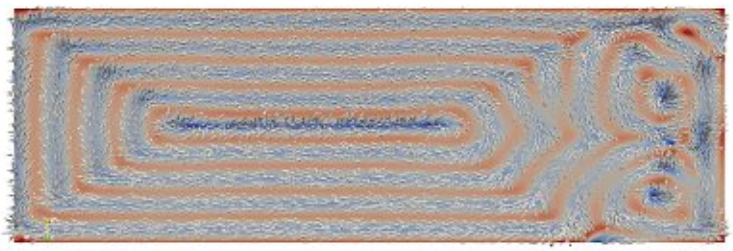

(b) Relaxed structure

Figure 38: A starting configuration as seen in (a) leads to a closed flux structure in the form of a vortex (b) due to the demagnetization energy, as can be found in the experiment.

As a final test to compare the experimental data with the simulations, an attempt is made to obtain simulations that represent one-to-one the experimental MFM images. The experimental $H_{\mathrm{stray,z}}$ values are taken as start parameters. Then the starting $M_{\mathrm{z}}$ is set to be $+0.5\ M_{\mathrm{s}}$ if $H_{\mathrm{stray,z}}$ is positive and $-0.5\ M_{\mathrm{s}}$ if it is negative. $M_{\mathrm{y}}$ and $M_{\mathrm{x}}$ is held constant at $0.87\ M_{\mathrm{s}}$ and $0\ M_{\mathrm{s}}$ respectively. A simulation with a 100 nm thick structure shows a relaxed structure astonishingly close to the MFM image. The same procedure but with experimental data from a 42 nm structure exposed an unexpected result. The relaxed structure does not retains its shape of stripes that all look more or less in one direction, similar to Fig. 39a. Instead, it relaxes into a configuration with a vortex structure (Fig 40). One possible reason for this behavior could be the fact that the stripes from the 42 nm sample are less homogeneous than those from Fig. 39a and therefore not so stable.

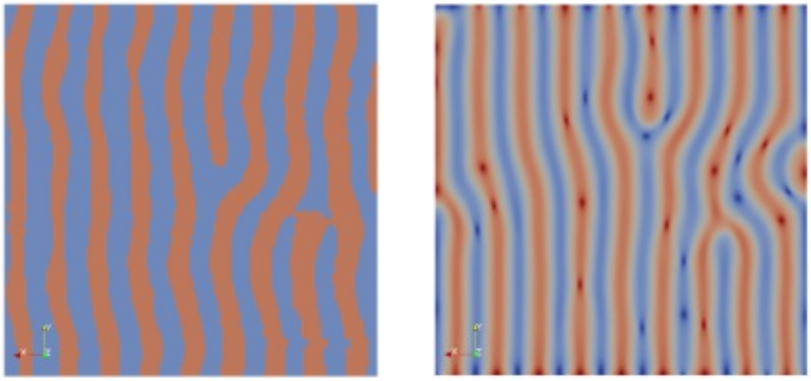

(a) Starting configuration (b) Relaxed structure

Figure 39: $M_{\mathrm{z}}$ of a $1600 \times 1600 \times 100$ nm Structure. The starting configuration was acquired from experimental MFM images.



Die approbierte gedruckte Originalversion dieser Diplomarbeit ist an der TU Wien Bibliothek verfügbar
The approved original version of this thesis is available in print at TU Wien Bibliothek.
TU Bibliothek Your knowledge hub WIEN

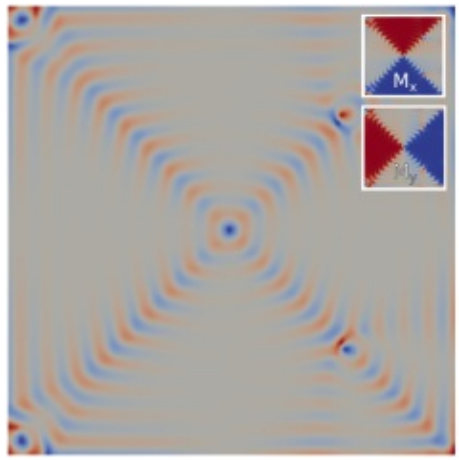


Figure 40: A $950 \times 950 \times 42$ nm film shows a vortex domain wall in the magnetization configuration. The stripes are displayed through the color coding of the $m_z$ component. $m_y$ and $m_x$ are color coded in the inset.

# 6 Co/Ni-Co

A study by Jonas Zehner et al. [28], on $[Co/Ni]_4$ multilayers has shown a spin reorientation transition from perpendicular to in-plane magnetization upon increasing a top Co layer. Micromagnetic simulations are performed for comparison and to determine the critical Co layer thickness at which the switch occurs.

## 6.1 Calculations of the critical thickness

This section shows the calculation of the critical thickness of the cobalt layer at which the magnetization switches from in-plane to perpendicular. For that purpose the demagnetization field, as well as the anisotropy field, have to be taken into account. For a system with an infinitely large surface, the energy contribution of the demagnetization field can be calculated with (10) to be

$$E^{\perp}_{\text{demag}} = \frac{\mu_0}{2} M_s^2 V \quad \text{and} \quad E^{\parallel}_{\text{demag}} = 0, \tag{27}$$

where $E^{\perp}_{\text{demag}}$ is the out of plane and $E^{\parallel}_{\text{demag}}$ is the in-plane demagnetization energy and $V$ represents for the volume of the system. For the same system as above the anisotropy energy can be expressed as

$$E^{\perp}_{\text{aniso}} = -K_1 V \quad \text{and} \quad E^{\parallel}_{\text{aniso}} = 0. \tag{28}$$



Die approbierte gedruckte Originalversion dieser Diplomarbeit ist an der TU Wien Bibliothek verfügbar
The approved original version of this thesis is available in print at TU Wien Bibliothek.
TU Bibliothek Your knowledge hub WIEN

With Eq. (27) and (11) the total areal energy density for these two fields can be calculated to be

$$\varepsilon^{\perp}_{\text{total}} = (\frac{\mu_0}{2} M_{\text{s}}^2 - K_1)\ D \quad \text{and} \quad \varepsilon^{\parallel}_{\text{total}} = 0, \tag{29}$$

where $D$ is the thickness of the structure. The simulated structure consists of two layers with different saturation magnetization and anisotropy constants, on top of each other. Therefore the perpendicular surface energy density and further with $\varepsilon^{\perp}_{\text{total}} = 0$ the critical thickness ratio for the structure can be calculated to be

$$\varepsilon^{\perp}_{\text{total}} = (\frac{\mu_0}{2} M_{\text{s},1}^2 - K_{1,1})\ D_1 + (\frac{\mu_0}{2} M_{\text{s},2}^2 - K_{1,2})\ D_2 \tag{30}$$

and

$$\frac{D_2}{D_1} = -\frac{\mu_0 M_{\text{s},1}^2 - 2K_{1,1}}{\mu_0 M_{\text{s},2}^2 - 2K_{1,2}}. \tag{31}$$

The indices 1 and 2 stand for the lower and upper layers respectively.

## 6.2 One dimensional simulation

For the first simulation approach a one-dimensional setup is chosen. The software magnum.fe was used to perform the simulations of the Co/Ni-Co structure. This structure is composed of four Co/Ni layers with $D_{\text{Co}} = 0.21$ nm and $D_{\text{Ni}} = 0.6$ nm, which adds up to a total thickness of $D_1 = 3.24$ nm for the Co/Ni multi-layers. The radius of the simulated sample is $R = 2$ nm. On top of this structure is a Co layer with varying thickness. As material parameters for the Ni/Co layer, $M_{\text{s}} = 600 \times 10^3$ A/m, $A = 1.1 \times 10^{-11}$ J/m and $K_1 = 3.64 \times 10^5$ J/m$^3$ with easy axis z is selected. The cobalt layer has material parameters of $M_{\text{s}} = 14 \times 10^5$ A/m, $A = 30 \times 10^{-12}$ J/m and $K_1 = 2.1 \times 10^5$J/m$^3$, again with easy axis z. The starting magnetization distribution is set homogeneously perpendicular. The relaxation of the system is simulated with the consideration of exchange field and anisotropy field. In order to account for the lateral dimension of the sample, the effect of the demagnetization field is considered in terms of an additional easy-plane contribution to the anisotropy energy. Therefore the effective anisotropy constant

$$K_{\text{eff}} = K_1 - \left(\frac{\mu_0 M_{\text{s}}^2}{2}\right) \tag{32}$$

was used. This leads to $k_{\text{eff, CoNi}} = 1.378 \times 10^5$ J/m$^3$ and $k_{\text{eff, Co}} = -1.022 \times 10^6$ J/m$^3$. As expected from experiment, a critical thickness at which the magnetization distri-



Die approbierte gedruckte Originalversion dieser Diplomarbeit ist an der TU Wien Bibliothek verfügbar
The approved original version of this thesis is available in print at TU Wien Bibliothek.
TU Bibliothek Your knowledge hub WIEN

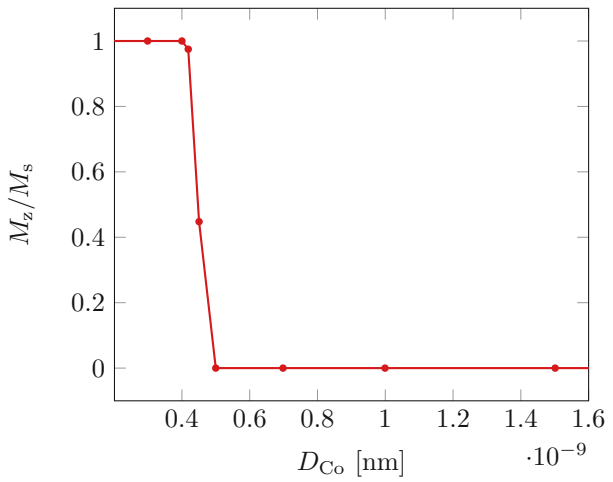


Figure 41: $M_z/M_s$ for different Co layer thicknesses. The simulated structure consists of a cylindrical Co layer on top of a $[Co/Ni]_4$ multi-layer with radius $R = 2$ nm .

bution switches from perpendicular to in-plane is found. In the simulation the magnetization remains perpendicular for a cobalt layer thickness beneath 0.42 nm. At a thickness of 0.42 nm and 0.45 nm the magnetizations is tilted and switches to in-plane above that. A plot of $M_z/M_s$ is shown in Fig. 41. Figure 42 shows images of the relaxed Co/Ni-Co structure with a cobalt layer thickness of 0.38 nm, 0.45 nm and 0.5 nm. To compare the results of the simulation with the analytic value the material parameters are inserted into Eqn. 31. With a thickness of 3.24 nm for the Co/Ni layer and with (31) the calculated critical Co layer thickness is $D_{co} = 0.437$ nm. The simulated critical Co layer thickness in the range of 0.45 nm is already in the range of the analytic value but is too small when compared with the experiment. This discrepancy pointed Jonas Zehner et al. [28] to the influence of an on top cobalt oxide layer on the measured critical thickness. After taking into account the oxide layer, the simulation agrees well with the experimental observation.



Die approbierte gedruckte Originalversion dieser Diplomarbeit ist an der TU Wien Bibliothek verfügbar
The approved original version of this thesis is available in print at TU Wien Bibliothek.
TU Bibliothek Your knowledge hub WIEN

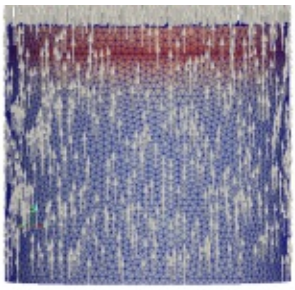

(a) $D_{\mathrm{Co}} = 0.38$ nm

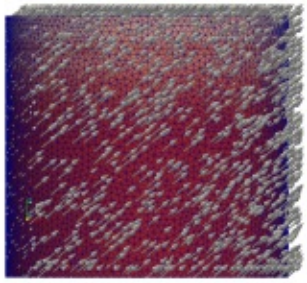

(b) $D_{\mathrm{Co}} = 0.45$ nm

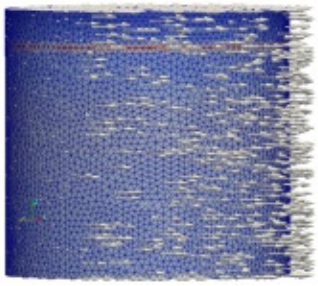

(c) $D_{\mathrm{Co}} = 0.5$ nm

Figure 42: Magnetization distribution of a cylindrical structure with radius $R = 2$ nm and easy axis z. The structure is simulated as a $[\mathrm{Co/Ni}]_4$ multi-layer with 3.24 nm thickness and a Co layer with varying thickness on top of it. The material parameters are $M_{\mathrm{s}} = 600 \times 10^3$ A/m, $A = 1.1 \times 10^{-11}$ J/m and $K_{\mathrm{eff,\ CoNi}} = 1.378 \times 10^5$ J/m$^3$ for the $[\mathrm{Co/Ni}]_4$ multilayer and $M_{\mathrm{s}} = 14 \times 10^5$ A/m, $A = 30 \times 10^{-12}$ J/m and $K_{\mathrm{eff,\ Co}} = -1.022 \times 10^6$J/m$^3$ for the Co layer. The effective anisotropy constants consider the effect of the demagnetization field and are calculated with Eqn. (32).



Die approbierte gedruckte Originalversion dieser Diplomarbeit ist an der TU Wien Bibliothek verfügbar
The approved original version of this thesis is available in print at TU Wien Bibliothek.
TU Bibliothek Your knowledge hub WIEN

## 6.3 Simulating the Co/Ni-Co Structure as one layer

To simplify the simulations while maintaining the representative nature of the experiment, the Co/Ni-Co structure is simulated as one homogeneous layer with effective values for the saturation magnetization, the anisotropy constant and the exchange constant. This simplification makes it easier to simulate structures with larger dimensions. The effective values are calculated with,

$$M_{\text{eff}} = \frac{M_{\text{s},1}D_1 + M_{\text{s},2}D_2}{D_{\text{tot}}}, \tag{33}$$

$$A_{\text{eff}} = \frac{A_{\text{s},1}D_1 + A_{\text{s},2}d_2}{D_{\text{tot}}}, \tag{34}$$

and

$$K_{1,\text{eff}} = \frac{1}{D_{\text{tot}}}(K_{1,1}D_1 - \frac{1}{2}M_{\text{s},1}^2\mu_0 D_1 + K_{1,2}D_2 - \frac{1}{2}M_{\text{s},2}^2\mu_0 D_2) + M_{\text{s,eff}}^2\mu_0, \tag{35}$$

where the index 1 and 2 stand for the Co/Ni and the top Co layer and $D_{\text{tot}} = D_1 + D_2$. Therefore the effective values are $D_{\text{tot}} = 3.79$ nm, $M_{\text{s,eff}} = 716 \times 10^3$ A/m, $A_{\text{eff}} = 1.38 \times 10^{-11}$ J/m and $K_{1,\text{eff}} = 2.92 \times 10^5$ J/m$^3$. The simulations with these effective parameters are performed on two different structures, a cylindrical structure in analogy with the previous simulation but with the consideration of the stray-field and on a cuboid structure with periodical boundary conditions. The implementation of periodic boundary conditions leads to the use of magnum.fd as the simulation software. The cylindrical structure has a critical thickness around 0.5 nm which is slightly above the analytical value of $D_{\text{Co,crit}} = 0.437$ nm (Fig. 43).

Due to boundary effects the relaxed structures with a thickness in range of $D_{\text{Co,crit}}$ have an inhomogeneous magnetization distribution as shown in Fig. 44. A critical thickness even closer to the analytical value is obtained with periodical boundary conditions in the direction of the x- and y-axis and with implementing the stray-field. Figure 45 shows a sharp edge in the magnetizations z component at a cobalt layer thickness of 0.437 nm.

For this structure and again with effective parameters Eqn. (33- 35) hysteresis curves with different Co layer thicknesses are simulated. Therefore an external perpendicular or in-plane magnetic field is ramped while the corresponding magnetization component is recorded. The simulated magnetization curves can be seen in Fig. 46. Underneath the critical thickness a perpendicular hysteresis can be measured clearly. The coercivity of this hysteresis loop is shrinking as $D_{\text{crit}}$ is approached from below. However



Die approbierte gedruckte Originalversion dieser Diplomarbeit ist an der TU Wien Bibliothek verfügbar
The approved original version of this thesis is available in print at TU Wien Bibliothek.
TU Bibliothek Your knowledge hub WIEN

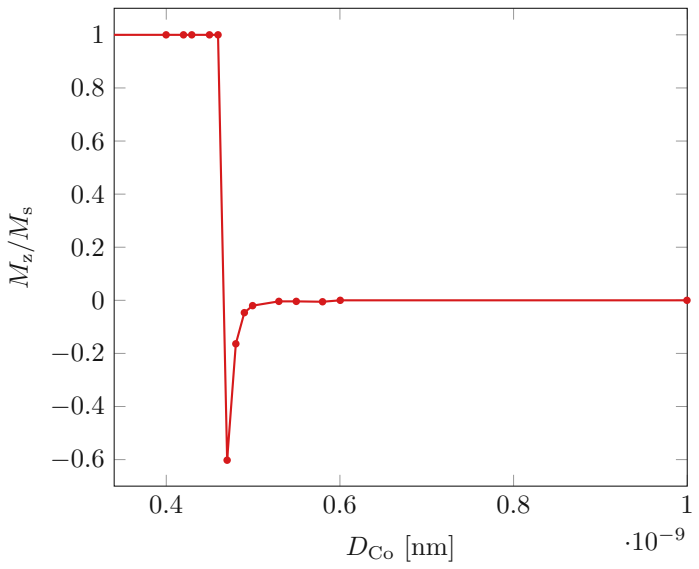


Figure 43: The plot shows the normalized $M_z$ versus $D_{Co}$ for a cylindrical Co/Ni-Co structure with $R = 250$ nm. The structure was simulated as one layer with effective material parameters calculated with Eqn. (33-35).

there is no in-plane hysteresis underneath $D_{crit}$ as $M/M_s$ is in- and decreasing linearly with the external field. At the critical thickness the hysteresis loop for the perpendicular configuration is very tight with a coercivity about 0.13 $\mu_0$mT. The in-plane magnetization rises or falls evenly with the field, but shows a slight hysteresis at the corners to saturation. For larger thicknesses there is no in-plane hysteresis and the magnetization switches between $-M_s$ and $+M_s$ depending on the sign of the field. The perpendicular contribution shows a similar form but with greater saturation field as the in-plane curve at $D_{crit}$. The saturation field for the perpendicular configuration increases with the thickness.



Die approbierte gedruckte Originalversion dieser Diplomarbeit ist an der TU Wien Bibliothek verfügbar
The approved original version of this thesis is available in print at TU Wien Bibliothek.
TU Bibliothek Your knowledge hub WIEN

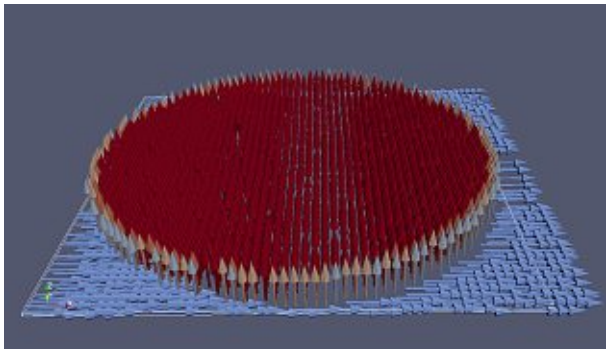

a: $D_{\mathrm{Co}} = 0.46$ nm

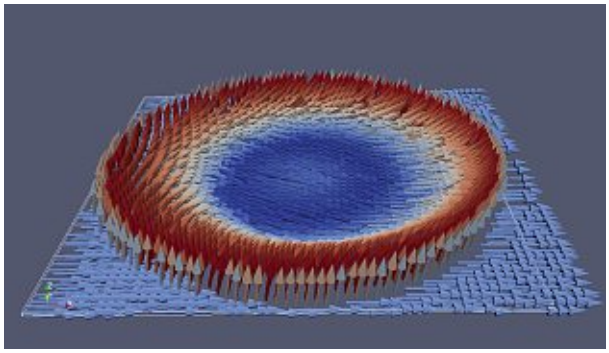

b: $D_{\mathrm{Co}} = 0.48$ nm

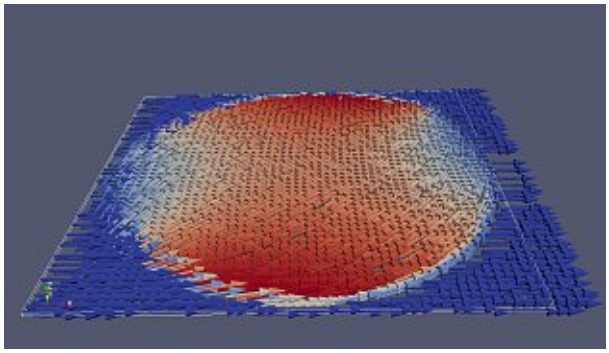

c: $D_{\mathrm{Co}} = 1$ nm

Figure 44: Magnetization distribution of a cylindrical Co/Ni-Co structure with $R = 250$ nm. The Co layer thickness is underneath (a), near (b) and above (c) the critical thickness. The simulations are performed as one layer with effective material parameters and with the consideration of the stray-field.



Die approbierte gedruckte Originalversion dieser Diplomarbeit ist an der TU Wien Bibliothek verfügbar
The approved original version of this thesis is available in print at TU Wien Bibliothek.
TU Bibliothek Your knowledge hub WIEN

Die approbierte gedruckte Originalversion dieser Diplomarbeit ist an der TU Wien Bibliothek verfügbar
The approved original version of this thesis is available in print at TU Wien Bibliothek.
TU Bibliothek Your knowledge hub WIEN

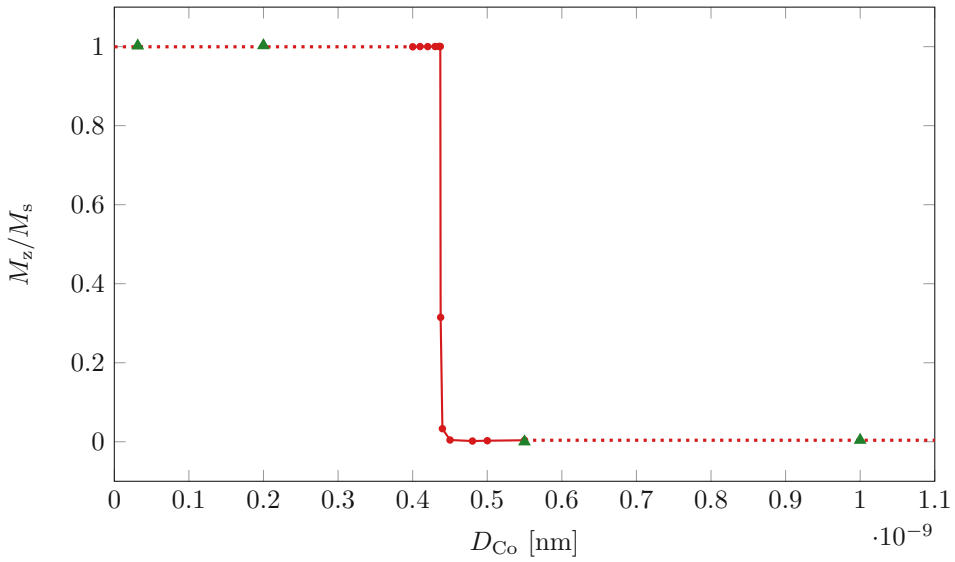


Figure 45: Normalized $M_z$ versus $D_{Co}$ for a cuboid Co/Ni-Co structure with PBC in the plane. The structure is simulated as one layer with effective material parameters. The triangles are representing experimentally obtained values [28], while the red dots are the simulated values. The solid and dotted lines are added to guide the eye.

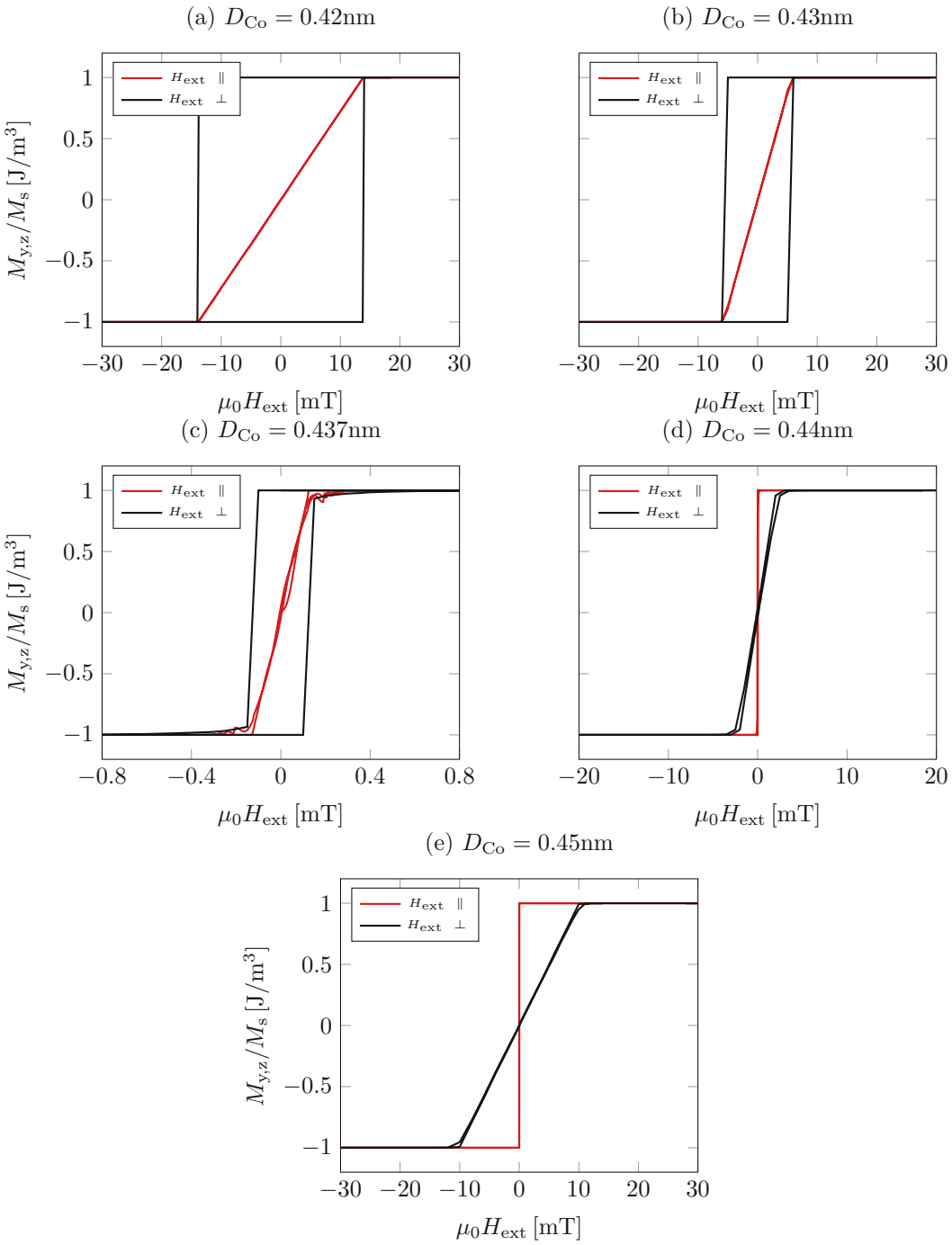


Figure 46: Hysteresis curves for a CO/Ni-Co structure with a Co layer thickness underneath, at and above the critical thickness. The structure is simulated as one cuboid layer with effective material parameters and PBC in the plane.

Die approbierte gedruckte Originalversion dieser Diplomarbeit ist an der TU Wien Bibliothek verfügbar
The approved original version of this thesis is available in print at TU Wien Bibliothek.
TU Bibliothek Your knowledge hub WIEN

# 7 Conclusions

The simulations on the Fe-Co-C structure reproduce the initial experiments for a large part. A method with relatively little computational effort was found to determine the width of strip domains, independent of the planar dimensions of the structure. The simulated stripe period over a wide range of thicknesses was in good agreement to the experimental results. In addition, the simulations were able to determine the effect of material parameters $A$ and $K_{\mathrm{u}}$ on the strip thickness and on the stray field. However, the absolute values of the stray field from simulation and experiment do not agree well. In addition, the simulations could not find the reason for the fluctuations of the stray field as well as the period occurring in the experiment. Further micromagnetic simulations in comparison with experimental investigations on other materials with well known material parameters could reveal, whether the quantitative comparison of the stray field is reasonable. The critical thickness, at which the reorientation phase from in-plane magnetization to a magnetization with dense stripe domains takes place, could be determined to be 42 nm for the Fe-Co-C layer. Moreover, the influence of the anisotropy constant on this critical length has been evaluated. The calculated single domain size of the Fe-Co-C material of 9.97 times the exchange length can be well classified with literature values for similar $Q$ values. A comparison to the observation of the stripes using analytical theory has shown that at the current state of time micromagnetic simulations are the method of choice to describe stripe domains. Since simulations with increased $K_1$ have shown that stripe domains are formed even above $K_1 = 0.58$ MJ/m$^3$, it is unlikely that Fe-Co-C will find a use in storage media. However, it could be used in permanent magnets, as it does not contain rare earth elements. The experiments on the Co/Ni-Co structure, which gave the impulse to the second set of simulations in this work, could be reproduced qualitatively and quantitatively. The simulations have also shown a conversion from perpendicular to in-plane magnetization at a given cobalt thickness. This critical thickness could be determined at 0.437 nm, which indicated an oxide layer on the experimental sample. This not negligible oxide layer was then found by the group of [28]. An analytical formula was derived, the result of which corresponds extremely well to the thickness obtained in the simulations. In addition, the different simulation methods showed the validity of simulating a structure consisting of several different layers as one film of a



Die approbierte gedruckte Originalversion dieser Diplomarbeit ist an der TU Wien Bibliothek verfügbar
The approved original version of this thesis is available in print at TU Wien Bibliothek.
TU Bibliothek Your knowledge hub WIEN

single material with effective material parameters.

Die approbierte gedruckte Originalversion dieser Diplomarbeit ist an der TU Wien Bibliothek verfügbar
The approved original version of this thesis is available in print at TU Wien Bibliothek.

# References


[1] V. Neu, L. Reichel, and S. Fähler, "In private contact: Stripe domains in tetragonally distorted fe-co-c films with perpendicular anisotropy,"

[2] T. Burkert, L. Nordström, O. Eriksson, and O. Heinonen, "Giant magnetic anisotropy in tetragonal feco alloys," *Phys. Rev. Lett.*, vol. 93, p. 027203, Jul 2004.

[3] D. Suess, T. Schrefl, S. Fähler, M. Kirschner, G. Hrkac, F. Dorfbauer, and J. Fidler, "Exchange spring media for perpendicular recording," *Applied Physics Letters*, vol. 87, no. 1, p. 012504, 2005.

[4] T. Hasegawa, S. Kanatani, M. Kazaana, K. Takahashi, K. Kumagai, M. Hirao, and S. Ishio, "Conversion of feco from soft to hard magnetic material by lattice engineering and nanopatterning," *Scientific reports*, vol. 7, no. 1, pp. 1–7, 2017.

[5] Z. Wu, N. Huang, Z. Liu, J. Wu, W. Duan, B.-L. Gu, and X.-W. Zhang, "Ferroelectricity in $Pb(zr_{0.5}ti_{0.5})o_3$ thin films: Critical thickness and 180° stripe domains," *Phys. Rev. B*, vol. 70, p. 104108, Sep 2004.

[6] M. Ghidini, G. Zangari, I. L. Prejbeanu, G. Pattanaik, L. D. Buda-Prejbeanu, G. Asti, C. Pernechele, and M. Solzi, "Magnetization processes in hard co-rich co–pt films with perpendicular anisotropy," *Journal of Applied Physics*, vol. 100, no. 10, p. 103911, 2006.

[7] J. Brandenburg, R. Hühne, L. Schultz, and V. Neu, "Domain structure of epitaxial co films with perpendicular anisotropy," *Phys. Rev. B*, vol. 79, p. 054429, Feb 2009.

[8] M. Coïsson, F. Vinai, P. Tiberto, and F. Celegato, "Magnetic properties of fesib thin films displaying stripe domains," *Journal of Magnetism and Magnetic Materials*, vol. 321, no. 7, pp. 806 – 809, 2009. Proceedings of the Forth Moscow International Symposium on Magnetism.

[9] A. Hubert and R. Schäfer, *Magnetic Domains*. Springer Berlin Heidelberg New York, 1998.




Die approbierte gedruckte Originalversion dieser Diplomarbeit ist an der TU Wien Bibliothek verfügbar
The approved original version of this thesis is available in print at TU Wien Bibliothek.
TU Bibliothek Your knowledge hub WIEN

[10] G. Selke, B. Krüger, A. Drews, C. Abert, and T. Gerhardt, "magnum.fd." https://github.com/micromagnetics/, 2014.

[11] M. E. Schabes and H. N. Bertram, "Magnetization processes in ferromagnetic cubes," *Journal of Applied Physics*, vol. 64, no. 3, pp. 1347–1357, 1988.

[12] M. E. Schabes, "Micromagnetic theory of non-uniform magnetization processes in magnetic recording particles," *Journal of magnetism and magnetic materials*, vol. 95, no. 3, pp. 249–288, 1991.

[13] A. Aharoni and J. Jakubovics, "Cylindrical magnetic domains in small ferromagnetic spheres with uniaxial anisotropy," *Philosophical Magazine B*, vol. 53, no. 2, pp. 133–145, 1986.

[14] C. Kittel, "Theory of the structure of ferromagnetic domains in films and small particles," *Phys. Rev.*, vol. 70, no. 11, 12, 1946.

[15] R. Choksi, R. V. Kohn, and F. Otto, "Domain branching in uniaxial ferromagnets: a scaling law for the minimum energy," *Communications in mathematical physics*, vol. 201, no. 1, pp. 61–79, 1999.

[16] Y. Millev, "Bose - einstein integrals and domain morphology in ultrathin ferromagnetic films with perpendicular magnetization," *Journal of Physics: Condensed Matter*, vol. 8, pp. 3671–3676, may 1996.

[17] Z. Málek and V. Kamberský, "Theory of the structure of ferromagnetic domains in films and small particles," *Czech. J. Phys.*, vol. 8, 1958.

[18] R. Skomski, H.-P. Oepen, and J. Kirschner, "Micromagnetics of ultrathin films with perpendicular magnetic anisotropy," *Phys. Rev. B*, vol. 58, pp. 3223–3227, Aug 1998.

[19] Abert, Claas, "Micromagnetics and spintronics: models and numerical methods," *Eur. Phys. J. B*, vol. 92, no. 6, p. 120, 2019.

[20] W. Brown, *Micromagnetics, by w.f. brown.* Interscience, 1963.

[21] A. Holz and H. Kronmüller, "The nucleation of stripe domains in thin ferromagnetic films," *physica status solidi (b)*, vol. 31, no. 2, pp. 787–798, 1969.



Die approbierte gedruckte Originalversion dieser Diplomarbeit ist an der TU Wien Bibliothek verfügbar
The approved original version of this thesis is available in print at TU Wien Bibliothek.
TU Bibliothek Your knowledge hub WIEN

[22] J. Fidler and T. Schrefl, "Micromagnetic modelling-the current state of the art," *Journal of Physics D: Applied Physics*, vol. 33, no. 15, p. R135, 2000.

[23] P. Palmesi, L. Exl, F. Bruckner, C. Abert, and D. Suess, "Highly parallel demagnetization field calculation using the fast multipole method on tetrahedral meshes with continuous sources," *Journal of Magnetism and Magnetic Materials*, vol. 442, pp. 409–416, 2017.

[24] J. E. Miltat and M. J. Donahue, "Numerical micromagnetics: Finite difference methods," *Handbook of magnetism and advanced magnetic materials*, 2007.

[25] E. Fehlberg, "Low-order classical runge-kutta formulas with stepsize control and their application to some heat transfer problems," 1969.

[26] M.Kisielewski, A. Maziewski, and V. Zablotskii, "High cobalt layer thickness spin-reorientation phase transition," *Journal of Magnetism and Magnetic Materials*, vol. 316, pp. 277–280, 2007.

[27] M. Hehn, S. Padovani, K. Ounadjela, and J. Bucher, "Nanoscale magnetic domain structures in epitaxial cobalt films," *Physical Review B*, vol. 54, no. 5, p. 3428, 1996.

[28] J. Zehner, "In private contact: Tailoring magnetism in Co/[Co/Ni] multilayers by Co surface layer manipulation,"



Die approbierte gedruckte Originalversion dieser Diplomarbeit ist an der TU Wien Bibliothek verfügbar
The approved original version of this thesis is available in print at TU Wien Bibliothek.
TU Bibliothek Your knowledge hub WIEN